REAP: A platform to identify autoantibodies that target the human exoproteome

Eric Y. Wang[1,*], Yile Dai[1,*], Connor E. Rosen[1,*], Monica M. Schmitt[4], Mei X. Dong[3], Elise M. N. Ferré[4], Feimei Liu[1], Yi Yang[1], Jaime A. Gonzalez-Hernandez[1], Eric Meffre[1], Monique Hinchcliffe[3], Fotios Koumpouras[3], Michail S. Lionakis[4], Aaron M. Ring[1,2,#]

[1] Department of Immunobiology, Yale School of Medicine, New Haven, CT, USA
[2] Department of Pharmacology, Yale School of Medicine, New Haven, CT, USA
[3] Department of Internal Medicine, Yale School of Medicine, New Haven, CT, USA
[4] Fungal Pathogenesis Section, Laboratory of Clinical Immunology and Microbiology, National Institute of Allergy & Infectious Diseases, National Institutes of Health, Bethesda, MD, USA.

[*] These authors contributed equally to this work
[#] Correspondence: aaron.ring@yale.edu (A.M.R.)

Abstract

Autoantibodies that recognize extracellular proteins (the “exoproteome”) exert potent biological effects but have proven challenging to detect with existing screening technologies. Here, we developed Rapid Extracellular Antigen Profiling (REAP) as a technique for comprehensive, high-throughput discovery of exoproteome-targeting autoantibodies. With REAP, patient samples are applied to a genetically-barcoded library containing 2,688 human extracellular proteins displayed on the surface of yeast. Antibody-coated cells are isolated by magnetic selection and deep sequencing of their barcodes is used to identify the displayed antigens. To benchmark the performance of REAP, we screened 77 patients with autoimmune polyendocrinopathy candidiasis ectodermal dystrophy (APECED). REAP sensitively and specifically detected known autoantibody reactivities in APECED in addition to numerous previously unidentified reactivities. We further screened 106 patients with systemic lupus erythematosus (SLE) and identified novel autoantibody reactivities against a diverse set of antigens including growth factors, extracellular matrix components, cytokines, and immunomodulatory proteins. Several of these responses were associated with disease severity and specific clinical manifestations of SLE and exerted potent functional effects on cell signaling *ex vivo*. These findings demonstrate the utility of REAP to atlas the expansive landscape of exoproteome-targeting autoantibodies and their impacts on patient health outcomes.

Introduction

Autoantibodies play a major etiological role across a wide range of diseases spanning autoimmunity, cancer, metabolic dysfunction, cardiovascular disease, infectious diseases, and even neurological and neurodegenerative conditions[1–8]. Though autoantibodies are commonly associated with adverse effects, they can also exhibit disease-ameliorating functions that are beneficial to patients. For example, immunosuppressive anti-cytokine autoantibodies are associated with less severe disease in numerous autoimmune conditions[9,10]; similarly, anti-tumor specific and opsonizing antibodies are associated with better survival in cancer patients[11–13]. Thus, analogous to genetic mutations, autoantibodies may explain a significant fraction of the clinical and phenotypic variation seen between individuals. Discovery of novel functional autoantibody responses in patients therefore has the potential to uncover key etiologic factors and therapeutic targets similar to the study of human genetics.

Within the human proteome, a particularly important group of autoantibody targets are extracellular and secreted proteins (collectively, the “exoproteome”). Because antibodies are themselves large (150 kDa) secreted proteins, they are most likely to recognize and act upon targets that reside within the same extracellular compartment[14]. While state-of-the-art technologies such as protein/peptide microarrays, proteome-scanning libraries using phage (PhIP-seq) and bacterial display have enabled the discovery of novel autoantibodies in a variety of diseases[15–23], these systems have limited sensitivity to detect autoantibodies against extracellular targets. This is due in part to the inherent difficulty of working with extracellular proteins, which often have unique folding requirements that include signal peptide removal, disulfide bond formation, and post-translational modifications such as glycosylation. Many of these features are not captured by platforms that express proteins or peptides in prokaryotic systems. Similarly, technologies that rely on the use of peptide fragments are not able to detect autoantibodies that recognize “conformational” protein epitopes (*i.e.*, three dimensional epitopes present when a protein is folded into its native state). This limitation may significantly hamper autoantibody detection, since as many as 90% of antibodies recognize conformational epitopes as opposed to linear peptides[24].

95

96 Here, we describe Rapid Exoproteome Antigen Profiling (REAP), a new method to
97 discover functional antibodies against the exoproteome. REAP leverages yeast-display
98 technology to assess the presence of autoantibody responses to 2,688 extracellular
99 proteins present in patient serum or plasma samples through a next-generation
100 sequencing-based approach. We use REAP to screen a cohort of 77 APECED patients
101 and successfully identify known autoantibodies along with novel "public" (present in many
102 patients) and "private" (present in only a few patients) reactivities. We further apply REAP
103 to a cohort of 106 patients with SLE and identify autoantibodies targeting cytokines,
104 cytokine receptors, growth factors, extracellular matrix components, and
105 immunomodulatory cell surface proteins, and validate several of these reactivities through
106 orthogonal assays. In both SLE and APECED, we identify autoantibody responses that
107 are associated with disease severity and specific clinical disease manifestations. Finally,
108 we find that autoantibodies in SLE patients that target the co-inhibitory ligand PD-L2 and
109 the cytokine IL-33 have functional antagonist activity *ex vivo*. These results indicate that
110 REAP is broadly useful for the discovery of autoantibodies targeting the exoproteome and
111 that functional autoantibodies within patient populations may provide key insights into
112 disease pathogenesis and therapeutic approaches.

113

114 **Results**

115 **Development of Rapid Exoproteome Antigen Profiling**

116 To develop a system capable of detecting autoantibody responses against conformational
117 extracellular proteins, we elected to use yeast surface display to comprehensively sample
118 the human exoproteome (**Fig. 1a**). As eukaryotic cells, yeast contain several features that
119 enable them to express extracellular proteins, including endoplasmic reticulum
120 chaperones, glycosylation machinery, and disulfide bond proofreading systems[25].
121 Accordingly, a diverse range of mammalian extracellular protein families have been
122 successfully expressed with yeast display, including proteins with folds such as the
123 immunoglobulin superfamily (IgSF), TNF superfamily (TNFSF), TNF receptor superfamily
124 (TNFRSF), von Willebrand factor A (vWFA) domains, fibronectin domain, leucine-rich
125 repeat (LRR), EGF-like, insulin-like, cytokines, growth factors, and even complicated

126 assemblies like peptide:MHC complexes, T cell receptors, and intact antibodies[26–41]. We
127 therefore constructed a genetically-barcoded yeast-displayed exoproteome library of
128 approximately 2,700 human extracellular and secreted proteins. The library comprises
129 actively displayed proteins from a wide range of protein families and encompasses 87%
130 of all human exoproteins with extracellular regions from 50-600 amino acids in length
131 (**Fig. 1b, Supplementary Fig. 1a-c**). While there is within-library heterogeneity in
132 individual protein abundance and the number of unique barcodes associated with each
133 gene, the library is relatively uniform and the vast majority of proteins fall within a narrow
134 range suited to coverage by standard next-generation sequencing approaches (**Fig.**
135 **1c,d**). Full details on the design and composition of the library are described in the
136 Methods and in **Supplemental Table 1**.
137
138 We next optimized procedures for high-throughput identification of seroreactivities
139 against proteins in our exoproteome library for REAP (**Fig. 1d**). Briefly, IgG purified from
140 patient serum or plasma is incubated with the yeast library. Autoantibody-coated cells are
141 then isolated by magnetic separation and deep sequencing of the library-encoded DNA
142 barcodes is used to identify the corresponding antigens encoded by these cells. To
143 quantify the degree of antibody reactivity to a given antigen, we developed a custom
144 scoring algorithm ("REAP Score") based on the enrichment of each antigen's barcodes
145 after selection (see Methods). Screening of the exoproteome library with a set of nine
146 conformation-specific monoclonal antibodies against a variety of extracellular proteins
147 showed that all antibody targets were detected specifically and robustly (**Fig. 2a,b**). To
148 further assess the conformational nature of proteins displayed in the library, we performed
149 a REAP screen using a panel of 30 recombinant proteins with known binding partners in
150 the library. REAP accurately detected the cognate binding partners for each of these
151 proteins, with minimal enrichment of off-target proteins (**Fig. 2c**).
152
153 **Evaluation of REAP performance in APECED**
154 To evaluate the capacity of REAP to detect exoproteome-directed autoantibodies in
155 complex patient samples such as polyclonal responses in serum, we screened a cohort
156 of 77 APECED patients (**Supplementary Table 2**). APECED, also known as autoimmune

157 polyglandular syndrome type-1 (APS-1), is a rare genetic autoimmune disease caused
158 by mutations in the autoimmune regulator (*AIRE*) gene, resulting in loss of central
159 tolerance and the development of chronic mucocutaneous candidiasis (CMC), severe
160 endocrinopathies and other nonendocrine autoimmune sequelae such as pneumonitis,
161 hepatitis, alopecia, vitiligo, and vitamin B12 deficiency/pernicious anemia[42]. Interestingly,
162 APECED patients harbor widespread and pathognomonic autoantibodies targeting
163 numerous cytokines including type I and type III interferons, IL-22, IL-17A, and IL-17F[43–
164 47]. REAP readily identified autoantibody responses against these cytokines in APECED
165 patient samples, but not in samples from healthy controls (**Fig. 3a**). Furthermore, the
166 frequencies of these autoreactivities in APECED patients closely matched the
167 frequencies determined from previous reports using gold-standard methodologies such
168 as enzyme-linked immunosorbent assay (ELISA) and luciferase immunoprecipitation
169 system immunoassay (LIPS) (**Fig. 3b**)[18,43,47]. We also identified autoantibodies against
170 gastric intrinsic factor (GIF), lipocalin-1 (LCN1), IL-5, IL-6, protein disulfide-isomerase-like
171 protein of the testis (PDILT), and BPI fold containing family member 1 and 2 (BPIFA1/2),
172 which have been previously described in APECED[18–21,48]. With respect to GIF reactivities,
173 the results seen with REAP demonstrated strong concordance with anti-GIF ELISA
174 results from the same patients (**Fig. 3c**).
175
176 To investigate the reproducibility of REAP, we compared $\log_2$[fold enrichment] between
177 technical (intra-assay) replicates across all APECED patient samples and found strong
178 positive correlations between replicates (median R^2 = 0.914; **Supplementary Fig. 1d**).
179 To investigate the sensitivity of REAP, we titrated varying amounts of IgG and performed
180 REAP and ELISA side-by-side for four autoantigens (**Supplementary Fig. 1e,f**). In each
181 case, REAP exhibited higher sensitivity than ELISA by 1-2 orders of magnitude, as seen
182 by the calculated EC_{50} values (**Fig. 3d**). Taken in aggregate, these data indicate that
183 REAP is capable of detecting known autoantibody responses against extracellular
184 proteins with high sensitivity and precision.
185
186 **APECED patients exhibit broad exoproteome-targeting autoantibody reactivities**
187

188 Previous reports using protein microarrays and PhIP-seq have shown that APECED
189 patients have greatly elevated numbers of autoantibody reactivities at a proteome-scale
190 compared to healthy controls. Analyzing the REAP data, we found that global
191 autoreactivity present in APECED also extends to the exoproteome (**Fig. 3e,**
192 **Supplementary Fig. 2a**). While some of the reactivities we observed have been
193 previously characterized, the screen also uncovered numerous previously undescribed
194 "public" (present in more than one patient) and "private" (present in only one patient)
195 reactivities. Two notable public reactivities were those against glycoprotein hormone
196 beta-5 (GPHB5), a thyrostimulin subunit, and pancreatic triacylglycerol lipase (PNLIP), a
197 tissue-restricted antigen that is regulated by AIRE in the thymus[49]. Using ELISA, we
198 confirmed the presence of autoantibody responses against these proteins and found that
199 the titers of autoantibodies were high, ranging from EC50s of approximately 1:100 to
200 1:10,000 (**Fig. 3f,g**). We additionally were able to correlate particular serological
201 responses to specific, variable clinical features of APECED. For example, we found that
202 autoantibodies against lipocalin-1 (LCN1) and BPIFA1, which had previously been
203 identified in APECED patients with Sjogren's-like syndrome[48], were enriched in a subset
204 of APECED patients with pneumonitis (6 out of 28 with pneumonitis), a life-threatening
205 non-endocrine complication of APECED, but universally negative in 49 patients without
206 pneumonitis or healthy controls (**Fig. 3h**). Of note, BPIFA1 reactivity was detected in a
207 patient with biopsy-proven pneumonitis without reactivity to the known lung-targeted
208 autoantibodies KCNRG and BPIFB1, which have an overall sensitivity of ~75% but are
209 negative in a quarter of patients with biopsy-proven pneumonitis[50]. Interestingly, the
210 single patient in our cohort with exocrine pancreatic insufficiency, a rare manifestation of
211 APECED[42], uniquely harbored reactivity to colipase (CLPS), an essential cofactor for
212 pancreatic lipase and related lipases (**Fig. 3a**)[51]. Thus, REAP enabled the detection of
213 novel autoantibody reactivities in the monogenic disease APECED, as well as
214 correlations of autoantibodies with clinical features of the disease.
215
216 **REAP identifies previously undescribed autoantibody reactivities in SLE patients**
217 We sought to apply REAP to study SLE, a systemic polygenic autoimmune disease
218 characterized by loss of tolerance to nucleic acids[52]. Though autoantibodies are a defining

219 feature in SLE, particularly those against nucleic acids and nuclear protein complexes[53],
220 the role of functional autoantibodies that target the exoproteome is less well established.
221 We thus performed REAP analysis on samples from a cohort of 106 SLE patients and 20
222 healthy controls. Patient and control demographics are shown in **Supplementary Table**
223 **3**. Compared to APECED, we found that exoproteome-targeting autoantibodies in SLE
224 patients were strikingly heterogeneous; though a wide variety of autoantigens were
225 identified, there were essentially no public autoantigens and most reactivities were
226 present in only a few patients (**Fig. 4a**). Several reactivities identified by REAP included
227 autoantigens that have previously been described in SLE such as IL-6, type I interferons,
228 IL-1α, and TNFα (including identification of a therapeutic anti-TNF antibody administered
229 to one of the patients). We further identified numerous novel autoantibodies targeting
230 other cytokines (*e.g.*, IL-4, IL-33), chemokines (*e.g.*, CXCL3, CCL8), growth factors (*e.g.*,
231 VEGF-B, FGF-21), extracellular matrix components (*e.g.*, epiphycan, vitrin), and
232 immunoregulatory cell surface proteins (*e.g.*, FAS, PD-L2, B7-H4).
233
234 To validate the large number of candidate autoantibody reactivities identified by REAP,
235 we tested autoantibody reactivities against several different proteins using LIPS and
236 ELISA and subsequently confirmed 16 of these autoantigens (**Table 1, Fig. 4f,i,**
237 **Supplementary Fig. 3a-h, j, n-r**). The subset of confirmed autoantibody reactivities
238 consisted of both shared and private reactivities and included examples of potentially
239 pathological and well as immunomodulatory reactivities, such as those against the
240 extracellular matrix component epiphycan (**Supplementary Fig. 3n**), the cytokine
241 receptor IL-18Rβ (**Supplementary Fig. 3p**), the death receptor FAS/TNFRSF6
242 (**Supplementary Fig. 3e**), the co-inhibitory ligand PD-L2 (**Fig. 4f**), and the IL-1 family
243 cytokine IL-33 (**Fig. 4i**). We additionally characterized the titers and IgG isotypes for
244 several of these responses, finding that they spanned a wide range of titers (1:10
245 to >1:10,000) and isotype classes (**Supplementary Fig. 3n-r, t-v**). Using these results,
246 as well as orthogonal validations of known APECED reactivities (**Supplementary Fig. 3i-**
247 **m**), we performed receiver operating characteristic (ROC) analysis to quantify the
248 performance of the REAP scoring algorithm. We found that REAP score sensitively and
249 specifically predicted autoantibody reactivity by ELISA and/or LIPS, with an area under

250 the curve (AUC) of 0.892 (**Supplementary Fig. 3s**). Because REAP exhibits greater
251 sensitivity for some antigens than the ELISA/LIPS "gold standards" (as was the case for
252 type I IFN autoantibodies in APECED), this number may represent a conservative
253 estimate of the true performance of REAP in predicting autoantibody reactivity.
254
255 **Exoproteome-targeting autoantibodies in SLE are functional and correlate with**
256 **disease severity**
257 Given the broad distribution of autoantibody responses in SLE, we wondered if particular
258 responses or patterns of reactivity were associated with specific clinical features of the
259 disease. At a global level, we found that the total numbers of autoantibody reactivities
260 identified with REAP correlated with worse clinical severity, as measured by the Systemic
261 Lupus Erythematosus Disease Activity Index (SLEDAI) score[54]. In particular, we found
262 that samples from patients with severe disease (SLEDAI score ≥ 9) had significantly
263 increased numbers of autoantibodies compared to healthy controls (**Fig. 4b,**
264 **Supplementary Fig. 2b**). Furthermore, SLE patients in all severity groups had reactivities
265 that were not observed in healthy individuals and these patterns of reactivity were
266 associated with particular SLE disease phenotypes. For instance, we found that
267 autoantibody reactivities against the chemokine CCL8, the cytokine IFN-alpha-6, and the
268 C-type lectin CD248 (endosialin) were significantly associated with hematuria and that
269 VEGF-B reactivities were associated with leukopenia (**Fig. 4c**). Additionally, patients
270 positive for CCL8 reactivity had significantly higher SLEDAI scores, indicating more
271 severe disease (**Fig. 4d**). By contrast, patients who exhibited autoreactivity against a set
272 of immunoregulatory proteins (PD-L2, RAET1E, CD44, B7H4, BTNL8, CD300E, IER3,
273 TNFRSF6, CD300LG, LILRB2, IGLL1, and LILRB4) had significantly lower SLEDAI
274 scores compared to patients negative for these autoantibodies (**Fig. 4e**).
275
276 Finally, we characterized the functionality of autoantibodies against two novel
277 autoantigens identified by REAP, PD-L2 and IL-33. As the primary biological function of
278 PD-L2 is mediated by its binding to its receptor PD-1, we tested whether autoantibodies
279 against PD-L2 could block this interaction. Serum samples from an SLE patient with anti-
280 PD-L2 autoantibodies were present at titers >1:100 and inhibited the interaction between

281 PD-L2 and PD-1 in a dose-dependent manner, while serum from a control patient without
282 anti-PD-L2 autoantibodies did not (**Fig. 4f-h**). To test the functional effects of anti-IL-33
283 autoantibodies, we used a HEK-Blue IL-33 reporter cell line, which produces secreted
284 alkaline phosphatase downstream of an NFκB promoter that is activated by the IL-33
285 pathway. Bulk IgG (isolated via protein G) from the SLE patient harboring anti-IL-33
286 autoantibodies potently neutralized IL-33 signaling with an IC_{50} less than 0.01 mg/mL,
287 while IgG from a control patient without anti-IL-33 autoantibodies had no neutralizing
288 effect (**Fig. 4i-k**). These findings underscore the ability of REAP to discover novel
289 autoantibodies with functional biological effects.
290
291 **Discussion**
292 In the present study we show that REAP is a sensitive and high-throughput platform for
293 discovery of exoproteome-directed autoantibodies. By querying antigens in a
294 conformationally-active state, REAP enables identification of autoantibodies that are
295 difficult to detect, if not entirely invisible to other technologies. This was particularly
296 evident in our screen of APECED samples, as we found that REAP was considerably
297 more accurate in detecting a well-defined subset of known extracellular autoantigen
298 reactivities compared to protein arrays and phage-peptide display approaches.
299 Furthermore, REAP enabled the identification of numerous previously undescribed
300 autoantigens in APECED patients, a surprising finding given how extensively
301 autoantibodies have been studied in this patient population.
302
303 We also identified a large set of previously undescribed autoantibody reactivities against
304 the exoproteome in SLE patients, a considerably more heterogeneous population than
305 APECED. The vast majority of these novel autoreactivities were relatively private with a
306 prevalence of <5% and in some cases present in only a single patient. Though these
307 autoantibody responses are rare, our studies suggest that they can exert large biological
308 effects that could meaningfully impact disease progression, akin to the effect of rare
309 genetic variants. For example, we identified a single SLE patient with mild disease activity
310 (SLEDAI score of 1) who had extraordinarily high-titer autoantibodies against IL-33 that
311 potently neutralized IL-33 signaling *in vitro*. This suggests that these IL-33 antibodies may

312 have played a protective role that ameliorated the severity of the disease in this individual
313 and, by extension, that IL-33 blockade could represent a potential therapeutic strategy in
314 SLE. Indeed, circulating IL-33 concentrations are elevated in SLE patients and are
315 positively correlated with C-reactive protein concentrations and clinical manifestations
316 such as thrombocytopenia and erythrocytopenia[55,56]. Similarly, preclinical studies in
317 mouse models have demonstrated that IL-33 exposure is associated with autoantibody
318 production and that neutralization of IL-33 suppresses lupus-like disease[57,58]. Beyond IL-
319 33, we also found that SLE patients with autoreactivity against a set of immunoreceptors
320 had substantially lower disease severity, indicating that disruption of those pathways
321 and/or opsonization of cells that express the receptors could similarly exert a protective
322 effect. Future investigation is warranted to determine the prevalence of these
323 autoantibodies in SLE patients and their potential protective effects on a larger,
324 confirmatory cohort. Nevertheless, our finding that functional autoantibodies responses
325 are highly variable between patients underscores the need for technologies like REAP
326 that can provide comprehensive, unbiased antibody profiling for large numbers of
327 patients. Without sufficient sample throughput and representation of the exoproteome,
328 these rare, but impactful autoantibody responses might not be readily detected.
329
330 REAP does have important limitations. While our data indicate that most exoproteome
331 antigens are displayed on the surface of yeast and we additionally demonstrated that
332 dozens of the library members are biochemically active (via recapitulating known binding
333 interactions), not all members of the exoproteome can be expressed in the yeast system.
334 This may be due to lack of specific chaperones, expression partners, or post-translational
335 modifications required for protein folding and activity. Furthermore, while yeast do perform
336 O- and N- linked glycosylation, their glycosylation patterns are characterized by a
337 hypermannose structure that is highly divergent from glycosylation seen in humans[59].
338 Thus, autoantibodies recognizing specific glycoforms of their antigens would not be
339 detected with REAP. Further improvement in the REAP platform could therefore involve
340 yeast strain engineering to co-express mammalian chaperone proteins to enhance folding
341 of human antigens and glycosylation enzymes to produce more human-like glycosylation
342 patterns, as has been described for the yeast species *Pichia pastoris*[60].

343

344 Though we initially applied REAP to the study of autoimmune conditions, an intriguing
345 avenue of future study with REAP and other serological profiling technologies is to
346 characterize autoantibody responses in diseases such as cancer, infectious diseases,
347 and neurological conditions that are not considered to have a primarily autoimmune
348 etiology. Identification of disease-modifying antibody responses in such conditions could
349 implicate new molecular pathways that contribute to disease pathology as well as novel
350 therapeutic targets and molecular diagnostics. Furthermore, patient autoantibodies could
351 represent potential therapeutic agents themselves. Technologies such as REAP can
352 enable these discoveries by revealing the diverse landscape of functional autoantibody
353 responses that influence health and disease.

354

355 **Materials and Methods**

356 **Library production.**

357 *Library design.* An initial library of 3093 human extracellular proteins was assembled
358 based on protein domains, immunological functions, and yeast-display compatibility. The
359 extracellular portion of each protein was identified by manual inspection of topological
360 domains annotated in the SwissProt database (January 2018). For proteins with uncertain
361 topology, full sequences were run through SignalP 4, Topcons, and GPIPred to identify
362 most likely topologies. For proteins with multiple extracellular portions, in general the
363 longest individual region was chosen for initial amplification. cDNAs for chosen proteins
364 were purchased from GE Dharmacon or DNASU. The protein sequences were further
365 modified to match isoforms available in purchased cDNAs. An inventory of antigens
366 included in the library are compiled in supplementary table 1.

367

368 *Library construction.* A two-step PCR process was used to amplify cDNAs for cloning into
369 a barcoded yeast-display vector. cDNAs were amplified with gene-specific primers, with
370 the forward primer containing a 5' sequence (CTGTTATTGCTAGCGTTTTAGCA) and the
371 reverse primer containing a 5' sequence (GCCACCAGAAGCGGCCGC) for template
372 addition in the second step of PCR. PCR reactions were conducted using 1 μL pooled
373 cDNA, gene-specific primers, and the following PCR settings: 98 ºC denaturation, 58 ºC

374 annealing, 72 ºC extension, 35 rounds of amplification. 1 µL of PCR product was used for
375 direct amplification by common primers Aga2FOR and 159REV, and the following PCR
376 settings: 98 ºC denaturation, 58 ºC annealing, 72 ºC extension, 35 rounds of amplification.
377 PCR product was purified using magnetic PCR purification beads (AvanBio). 90 µL beads
378 were added to the PCR product and supernatant was removed. Beads were washed twice
379 with 200 µL 70% ethanol and resuspended in 50 µL water to elute PCR products from the
380 beads. Beads were removed from purified PCR products. The 15bp barcode fragment
381 was constructed by overlap PCR. 4 primers (bc1, bc2, bc3, bc4; sequences listed below)
382 were mixed in equimolar ratios and used as a template for a PCR reaction using the
383 following PCR settings: 98 ºC denaturation, 55 ºC annealing, 72 ºC extension, 35 rounds
384 of amplification. Purified product was reamplified with the first and fourth primer using
385 identical PCR conditions. PCR products were run on 2% agarose gels and purified by gel
386 extraction (Qiagen). Purified barcode and gene products were combined with linearized
387 yeast-display vector (pDD003 digested with EcoRI and BamHI) and electroporated into
388 JAR300 yeast using a 96-well electroporator (BTX Harvard Apparatus) using the following
389 electroporation conditions: Square wave, 500 V, 5 ms pulse, 2 mm gap. Yeast were
390 immediately recovered into 1 mL liquid synthetic dextrose medium lacking uracil (SDO -
391 Ura) in 96-well deep well blocks and grown overnight at 30°C. Yeast were passaged once
392 by 1:10 dilution in SDO-Ura, then frozen as glycerol stocks. To construct the final library,
393 2.5 µL of all wells were pooled and counted. A limited dilution of 300,000 clones was sub-
394 sampled and expanded in SDO-Ura. Expression was induced by passaging into synthetic
395 galactose medium lacking uracil (SGO-Ura) at a 1:10 dilution and growing at 30°C
396 overnight. 10^8 yeast were pelleted and resuspended in 1 mL PBE (PBS with 0.5% BSA
397 and 0.5 mM EDTA) containing 1:100 anti-FLAG PE antibody (BioLegend). Yeast were
398 stained at 4° for 75 minutes, then washed twice with 1 mL PBE and sorted for FLAG
399 display on a Sony SH800Z cell sorter. Sorted cells were expanded in SDO-Ura
400 supplemented with 35 µg/mL chloramphenicol, expanded, and frozen as the final library.
401 **bc1**-TTGTTAATATACCTCTATACTTTAACGTCAAGGAGAAAAAACCCCGGATC
402 **bc2**-
403 CTGCATCCTTTAGTGAGGGTTGAANNNNNNNNNNNNNNNNTTCGATCCGGGGTTTTT
404 TCTCCTTG

405 **bc3**-
406 TTCAACCCTCACTAAAGGATGCAGTTACTTCGCTGTTTTTCAATATTTTCTGTTATTG
407 C
408 **bc4**-TGCTAAAACGCTAGCAATAACAGAAAATATTGAAAAACAGCG
409
410 *Barcode identification.* Barcode-gene pairings were identified using a custom Tn5-based
411 sequence approach. Tn5 transposase was purified as previously described, using the on-
412 column assembly method for loading oligos[61]. DNA was extracted from the yeast library
413 using Zymoprep-96 Yeast Plasmid Miniprep kits or Zymoprep Yeast Plasmid Miniprep II
414 kits (Zymo Research) according to standard manufacturer protocols. 5 µL of purified
415 plasmid DNA was digested with Tn5 in a 20 µL total reaction as previously described. 2
416 µL of digested DNA was amplified using primers index1 and index2, using the following
417 PCR settings: 98 ºC denaturation, 56 ºC annealing, 72 ºC extension, 25 rounds of
418 amplification. The product was run on a 2% gel and purified by gel extraction (Qiagen).
419 Purified product was amplified using primers index3 and index4, using the following PCR
420 settings: 98 ºC denaturation, 60 ºC annealing, 72 ºC extension, 25 rounds of amplification.
421 In parallel, the barcode region alone was amplified using primers index1 and index5,
422 using the following PCR settings: 98 ºC denaturation, 56 ºC annealing, 72 ºC extension,
423 25 rounds of amplification. The product was run on a 2% gel and purified by gel extraction
424 (Qiagen). Purified product was amplified using primers index3 and index6, using the
425 following PCR settings: 98 ºC denaturation, 60 ºC annealing, 72 ºC extension, 20 rounds
426 of amplification. Both barcode and digested fragment products were run on a 2% gel and
427 purified by gel extraction (Qiagen). NGS library was sequenced using an Illumina MiSeq
428 and Illumina v3 MiSeq Reagent Kits with 150 base pair single-end sequencing according
429 to standard manufacturer protocols. Gene-barcode pairings were identified using custom
430 code. Briefly, from each read, the barcode sequence was extracted based on the
431 identification of the flanking constant vector backbone sequences, and the first 25 bp of
432 sequence immediately following the constant vector backbone-derived signal peptide
433 were extracted and mapped to a gene identity based on the first 25 bp of all amplified
434 cDNA constructs. The number of times each barcode was paired with an identified gene
435 was calculated. Barcode-gene pairings that were identified more than twice, with an

436 overall observed barcode frequency of greater than .0002% were compiled. For barcodes
437 with multiple gene pairings matching the above criteria, the best-fit gene was manually
438 identified by inspection of all barcode-gene pairing frequencies and, in general,
439 identification of the most abundant gene pairing. In the final library, 2,688 genes were
440 confidently mapped to 35,835 barcodes.
441
442 **Rapid Extracellular Antigen Profiling.**
443 *Antibody purification and yeast adsorption.* 20 µL protein G magnetic resin (Lytic
444 Solutions) was washed twice with 100 µL sterile PBS, resuspended in 50 µL PBS, and
445 added to 50 µL serum or plasma. Serum-resin mixture was incubated for three hours at
446 4 ºC with shaking. Resin was washed five times with 200 µL PBS, resuspended in 90 µL
447 100 mM glycine pH 2.7, and incubated for five minutes at room temperature. Supernatant
448 was extracted and added to 10 µL sterile 1M Tris pH 8.0 (purified IgG). Empty vector
449 (pDD003) yeast were expanded in SDO-Ura at 30 ºC. One day later, yeast were induced
450 by 1:10 dilution in SGO-Ura for 24 hours. 10^8 induced yeast were washed twice with 200
451 µL PBE (PBS with 0.5% BSA and 0.5 mM EDTA), resuspended with 100 µL purified IgG,
452 and incubated for three hours at 4 ºC with shaking. Yeast-IgG mixtures were placed into
453 96 well 0.45 um filter plates (Thomas Scientific) and yeast-depleted IgG was eluted into
454 sterile 96 well plates by centrifugation at 3000 g for 3 minutes.
455
456 *Antibody yeast library selections.* Transformed yeast were expanded in SDO-Ura at 30
457 ºC. One day later, at an optical density (OD) below 8, yeast were induced by resuspension
458 at an OD of 1 in SGO-Ura supplemented with ten percent SDO-Ura and culturing at 30
459 ºC for 20 hours. Prior to selection, 400 µL pre-selection library was set aside to allow for
460 comparison to post-selection libraries. 10^8 induced yeast were washed twice with 200 µL
461 PBE and added to wells of a sterile 96-well v-bottom microtiter plate. Yeast were
462 resuspended in 100 µL PBE containing appropriate antibody concentration and incubated
463 with shaking for 1 hour at 4 ºC. Unless otherwise indicated, 10 µg antibody per well was
464 used for human serum or plasma derived antibodies and 1 µg antibody was used for
465 monoclonal antibodies. Yeast were washed twice with 200 µL PBE, resuspended in 100
466 µL PBE with a 1:100 dilution of biotin anti-human IgG Fc antibody (clone HP6017,

467 BioLegend) for human serum or plasma derived antibodies or a 1:25 dilution of biotin goat
468 anti-rat or anti-mouse IgG antibody (A16088, Thermo Fisher Scientific; A18869, Thermo
469 Fisher Scientific) for monoclonal antibodies. Yeast-antibody mixtures were incubated with
470 shaking for 30 minutes at 4 ºC. Yeast were washed twice with 200 µL PBE, resuspended
471 in 100 µL PBE with a 1:20 dilution of Streptavidin MicroBeads (Miltenyi Biotec), and
472 incubated with shaking for 30 minutes at 4 ºC. Yeast were then pelleted and kept on ice.
473 Multi-96 Columns (Miltenyi Biotec) were placed into a MultiMACS M96 Separator (Miltenyi
474 Biotec) and the separator was placed into positive selection mode. All following steps
475 were carried out at room temperature. Columns were equilibrated with 400 µL 70%
476 ethanol followed by 700 µL degassed PBE. Yeast were resuspended in 200 µL degassed
477 PBE and placed into the columns. After the mixture had completely passed through,
478 columns were washed three times with 700 µL degassed PBE. To elute the selected
479 yeast, columns were removed from the separator and placed over 96-well deep well
480 plates. 700 µL degassed PBE was added to each well of the column and the column and
481 deep well plate were spun at 50 g for 30 seconds. This process was repeated 3 times.
482 Selected yeast were pelleted, and recovered in 1 mL SDO -Ura at 30 ºC.
483
484 *Recombinant protein yeast library selections.* All pre-selection and yeast induction steps
485 were performed identically as those of the antibody yeast library selections. 10^8 induced
486 yeast were washed twice with 200 µL PBE and added to wells of a sterile 96-well v-bottom
487 microtiter plate. Yeast were resuspended in 100 µL PBE containing 75 µL clarified protein
488 expression supernatant and incubated with shaking for 1 hour at 4 ºC. Yeast were washed
489 twice with 200 µL PBE, resuspended in 100 µL PBE with 5 µL µMACS Protein G
490 MicroBeads (Miltenyi Biotec), and incubated with shaking for 30 minutes at 4 ºC. Selection
491 of yeast using the MultiMACS M96 Separator and subsequent steps were performed
492 identically as those of the antibody yeast library selections.
493
494 *Next generation sequencing library preparation and sequencing.* DNA was extracted from
495 yeast libraries using Zymoprep-96 Yeast Plasmid Miniprep kits or Zymoprep Yeast
496 Plasmid Miniprep II kits (Zymo Research) according to standard manufacturer protocols.
497 A first round of PCR was used to amplify a DNA sequence containing the protein display

498 barcode on the yeast plasmid. PCR reactions were conducted using 1 μL plasmid DNA,
499 159_DIF2 and 159_DIR2 primers (sequences listed below), and the following PCR
500 settings: 98 ºC denaturation, 58 ºC annealing, 72 ºC extension, 25 rounds of amplification.
501 PCR product was purified using magnetic PCR purification beads (AvanBio). 45 μL beads
502 were added to the PCR product and supernatant was removed. Beads were washed twice
503 with 100 μL 70% ethanol and resuspended in 25 μL water to elute PCR products from the
504 beads. Beads were removed from purified PCR products. A second round of PCR was
505 conducted using 1 μL purified PCR product, Nextera i5 and i7 dual-index library primers
506 (Illumina), and the following PCR settings: 98 ºC denaturation, 58 ºC annealing, 72 ºC
507 extension, 25 rounds of amplification. PCR products were pooled and run on a 1%
508 agarose gel. The band corresponding to 257 base pairs was cut out and DNA (NGS
509 library) was extracted using a QIAquick Gel Extraction Kit (Qiagen) according to standard
510 manufacturer protocols. NGS library was sequenced using an Illumina MiSeq and Illumina
511 v3 MiSeq Reagent Kits with 75 base pair single-end sequencing or using an Illumina
512 NovaSeq 6000 and Illumina NovaSeq S4 200 cycle kit with 101 base pair paired-end
513 sequencing according to standard manufacturer protocols. A minimum of 50,000 reads
514 per sample was collected and the pre-selection library was sampled at ten times greater
515 depth than other samples.
516 **159_DIF2**-
517 TCGTCGGCAGCGTCAGATGTGTATAAGAGACAGNNNNNNNNNNGAGAAAAAACCC
518 CGGATCG
519 **159_DIR2**-
520 GTCTCGTGGGCTCGGAGATGTGTATAAGAGACAGNNNNNNNNNNACGCTAGCAAT
521 AACAGAAAATATTG
522
523 *Data analysis.* REAP scores were calculated as follows. First, barcode counts were
524 extracted from raw NGS data using custom codes and counts from technical replicates
525 were summed. Next, aggregate and clonal enrichment was calculated using edgeR[62] and
526 custom codes. For aggregate enrichment, barcode counts across all unique barcodes
527 associated with a given protein were summed, library sizes across samples were
528 normalized using default edgeR parameters, common and tagwise dispersion were

529 estimated using default edgeR parameters, and exact tests comparing each sample to
530 the pre-selection library were performed using default edgeR parameters. Aggregate
531 enrichment is thus the log2 fold change values from these exact tests with zeroes in the
532 place of negative fold changes. Log2 fold change values for clonal enrichment were
533 calculated in an identical manner, but barcode counts across all unique barcodes
534 associated with a given protein were not summed. Clonal enrichment for a given reactivity
535 was defined as the fraction of clones out of total clones that were enriched (log2 fold
536 change ≥ 2). Aggregate (E_a) and clonal enrichment (E_c) for a given protein, a scaling
537 factor (β_u) based on the number of unique yeast clones (yeast that have a unique DNA
538 barcode) displaying a given protein, and a scaling factor (β_f) based on the overall
539 frequency of yeast in the library displaying a given protein were used as inputs to calculate
540 the REAP score, which is defined as follows.

541 $$\text{REAP score} = E_a * (E_c)^2 * \beta_u * \beta_f$$

542 β_u and β_f are logarithmic scaling factors that progressively penalize the REAP score of
543 proteins with low numbers of unique barcodes or low frequencies in the library. β_u is
544 applied to proteins with ≤ 5 unique yeast clones in the library and β_f is applied to proteins
545 with a frequency ≤ 0.0001 in the library. β_f was implemented to mitigate spurious
546 enrichment signals from low frequency proteins, which could occur due to sequencing
547 errors or stochasticity in the selection process. β_u was implemented because the clonal
548 enrichment metric is less valid for proteins with low numbers of unique yeast clones,
549 decreasing confidence in the validity of the reactivity. β_u and β_f are defined as follows
550 where x_u is the number of unique yeast clones for a given protein and x_f is the log10
551 transformed frequency of a given protein in the library.

552 $$\beta_u = \frac{\ln(x_u + 0.5)}{1.705}$$

553 $$\beta_f = \frac{\ln(x_f + 7.1)}{1.16}$$

554

555 **Recombinant protein production.**

556 *REAP recombinant protein production*. Proteins were produced as human IgG1 Fc
557 fusions to enable binding of secondary antibody and magnetic beads to the produced

558 proteins during the REAP process. Sequences encoding the extracellular portions of
559 proteins-of-interests that were present in the yeast display library were cloned by Gibson
560 assembly into a modified pD2610-v12 plasmid (ATUM). Modifications include addition of
561 an H7 signal sequence followed by a $(GGGGS)_3$ linker and a truncated human IgG1 Fc
562 (N297A). Protein-of-interest sequences were inserted directly downstream of the H7
563 leader sequence. Protein was produced by transfection into Expi293 cells (Thermo Fisher
564 Scientific) in 96-well plate format. One day prior to transfection, cells were seeded at a
565 density of 2 million cells per mL in Expi293 Expression Medium (Thermo Fisher
566 Scientific). In a 96-well plate, 0.5 µg plasmid DNA was diluted added to 25 µL Opti-MEM
567 (Thermo Fisher Scientific) and mixed gently. In a separate 96-well plate, 1.35 µL
568 ExpiFectamine was added to 25 µL Opti-MEM and mixed gently. The ExpiFectamine-
569 Opti-MEM mixture was added to the diluted DNA, mixed gently, and incubated for 20
570 minutes at room temperature. Expi293 cells were diluted to a density of 2.8 million cells
571 per mL and 500 µL of cells were added to each well of a 96-well deep well plate. 50 µL
572 of the DNA-ExpiFectamine-Opti-MEM mixture was added to each well. The plate was
573 sealed with Breathe-Easier sealing film (Diversified Biotech) and incubated in a humidified
574 tissue culture incubator (37 ºC, 8% CO_2) with shaking at 1,200 rpm so that cells were kept
575 in suspension. 18-20 hours post-transfection, 25 µL enhancer 2 and 2.5 µL enhancer 1
576 (Thermo Fisher Scientific) were added to each well. 4 days post-transfection, media was
577 clarified by centrifugation at 3000-4000 g for 5 minutes. Clarified media was used for
578 recombinant protein REAP.
579
580 *ELISA protein production.* Sequences encoding the extracellular portions of proteins-of-
581 interests that were present in the yeast display library were cloned by Gibson assembly
582 into pEZT_Dlux, a modified pEZT-BM vector. The pEZT-BM vector was a gift from Ryan
583 Hibbs (Addgene plasmid #74099). Modifications included insertion of an H7 Leader
584 Sequence followed by an AviTag (Avidity), HRV 3C site, protein C epitope, and an 8x his
585 tag. Protein-of-interest sequences were inserted directly downstream of the H7 leader
586 sequence. Protein was produced by transfection into Expi293 cells (Thermo Fisher
587 Scientific) according to standard manufacturer protocols. Transfected cells were
588 maintained according to manufacturer protocols. 4 days post-transfection, media was

589 clarified by centrifugation at 300 g for 5 minutes. Protein was purified from clarified media
590 by nickel-nitrilotriacetic acid (Ni-NTA) chromatography and desalted into HEPES buffered
591 saline + 100 mM sodium chloride, pH 7.5. Protein purity was verified by SDS-PAGE.
592
593 *Biotinylated protein production.* Sequences encoding the extracellular portions of
594 proteins-of-interests were cloned into pEZT_Dlux as described above. Protein was
595 expressed and purified as described above minus desalting. Enzymatic biotinylation with
596 BirA ligase was performed and protein was purified by size-exclusion fast protein liquid
597 chromatography using a NGC Quest 10 Chromatography System (Bio-Rad).
598
599 *LIPS protein production.* Sequences encoding Lucia luciferase (InvivoGen) fused by a
600 GGSG linker to the N-terminus of the protein-of-interest extracellular portion (as defined
601 above) were cloned by Gibson assembly into pEZT-BM. Protein was produced by
602 transfection into Expi293 cells (Thermo Fisher Scientific) according to standard
603 manufacturer protocols. Transfected cells were maintained according to manufacturer
604 protocols. 3 days post-transfection, media was clarified by centrifugation at 300 g for 5
605 minutes. Clarified media was used in luciferase immunoprecipitation systems assays.
606
607 **Enzyme-linked immunosorbent assays (ELISAs).**
608 200 or 400 ng of purchased or independently produced recombinant protein in 100 µL of
609 PBS pH 7.0 was added to 96-well flat bottom Immulon 2HB plates (Thermo Fisher
610 Scientific) and placed at 4 ºC overnight. Plates were washed once with 225 µL ELISA
611 wash buffer (PBS + 0.05% Tween 20) and 150 µL ELISA blocking buffer (PBS + 2%
612 Human Serum Albumin) was added to the well. Plates were incubated with shaking for 2
613 hours at room temperature. ELISA blocking buffer was removed from the wells and
614 appropriate dilutions of sample serum in 100 µL ELISA blocking buffer were added to
615 each well. Plates were incubated with shaking for 2 hours at room temperature. Plates
616 were washed 6 times with 225 µL ELISA wash buffer and 1:5000 goat anti-human IgG
617 HRP (Millipore Sigma) or anti-human IgG isotype specific HRP (Southern Biotech; IgG1:
618 clone HP6001, IgG2: clone 31-7-4, IgG3: clone HP6050, IgG4: clone HP6025) in 100 µL
619 ELISA blocking buffer was added to the wells. Plates were incubated with shaking for 1

620 hour at room temperature. Plates were washed 6 times with 225 µL ELISA wash buffer.
621 50 µL TMB substrate (BD Biosciences) was added to the wells and plates were incubated
622 for 15 minutes (pan-IgG ELISAs) or 20 minutes (isotype specific IgG ELISAs) in the dark
623 at room temperature. 50 µL 1 M sulfuric acid was added to the wells and absorbance at
624 450 nm was measured in a Synergy HTX Multi-Mode Microplate Reader (BioTek).
625
626 **Luciferase immunoprecipitation systems (LIPS) assays.**
627 Pierce Protein A/G Ultralink Resin (5 µL; Thermo Fisher Scientific) and 1 µL sample
628 serum in 100 µL Buffer A (50 mM Tris, 150 mM NaCl, 0.1% Triton X-100, pH 7.5) was
629 added to 96-well opaque Multiscreen HTS 96 HV 0.45 um filter plates (Millipore Sigma).
630 Plates were incubated with shaking at 300 rpm for 1 hour at room temperature.
631 Supernatant in wells was removed by centrifugation at 2000 g for 1 minute. Luciferase
632 fusion protein (10^6 RLU) was added to the wells in 100 µL Buffer A. Plates were incubated
633 with shaking at 300 rpm for 1 hour at room temperature. Using a vacuum manifold, wells
634 were washed 8 times with 100 µL Buffer A followed by 2 washes with 100 µL PBS.
635 Remaining supernatant in wells was removed by centrifugation at 2000 g for 1 minute.
636 Plates were dark adapted for 5 minutes. An autoinjector equipped Synergy HTX Multi-
637 Mode Microplate Reader (BioTek) was primed with QUANTI-Luc Gold (InvivoGen). Plates
638 were read using the following per well steps: 50 µL QUANTI-Luc Gold injection, 4 second
639 delay with shaking, read luminescence with an integration time of 0.1 seconds and a read
640 height of 1 mm.
641
642 **PD-L2 blocking assay.**
643 A single clone of PD-L2 displaying yeast was isolated from the library and expanded in
644 SDO-Ura at 30 ºC. Yeast were induced by 1:10 dilution into SGO-Ura and culturing at 30
645 ºC for 24 hours. 10^5 induced PD-L1 yeast were washed twice with 200 µL PBE and added
646 to wells of a 96-well v-bottom microtiter plate. Yeast were resuspended in 25 µL PBE
647 containing serial dilutions of sample serum and incubated with shaking for 1 hour at 4 ºC.
648 PD-1 tetramers were prepared by incubating a 5:1 ratio of biotinylated PD-1 and PE
649 streptavidin (BioLegend) for 10 minutes on ice in the dark. Yeast were washed twice with
650 200 µL PBE, resuspended in 25 µL PBE containing 10 nM previously prepared PD-1

651 tetramers, and incubated with shaking for 1 hour at 4 ºC. Yeast were washed twice with
652 200 µL PBE and resuspended in 75 µL PBE. PE fluorescent intensity was quantified by
653 flow cytometry using a Sony SA3800 Spectral Cell Analyzer. Percent max binding was
654 calculated based on fluorescent PD-1 tetramer binding in the absence of any serum.
655
656 **IL-33 neutralization assay.**
657 *IL-33 reporter cell line construction*. The full-length coding sequence for ST2 was cloned
658 by Gibson assembly into the lentiviral transfer plasmid pL-SFFV.Reporter.RFP657.PAC,
659 a kind gift from Benjamin Ebert (Addgene plasmid #61395). HEK-293FT cells were
660 seeded into a 6-well plate in 2 mL growth media (DMEM with 10% (v/v) FBS, 100 units/mL
661 penicillin, and 0.1 mg/mL streptomycin) and were incubated at 37°C, 5% CO2. Once cells
662 achieved 70-80% confluence approximately one day later, cells were transfected using
663 TransIT-LT1 (Mirus Bio) in Opti-MEM media (Life Technologies). TransIT-LT1 Reagent
664 was pre-warmed to room temperature and vortexed gently. For each well, 0.88 ug
665 lentiviral transfer plasmid along with 0.66 ug pSPAX2 (Addgene plasmid #12260) and
666 0.44 ug pMD2.G (Addgene plasmid #12259), kind gifts from Didier Trono, were added to
667 250 µL Opti-MEM media and mixed gently. TransIT-LT1 reagent (6 µl) was added to the
668 DNA mixture, mixed gently, and incubated at room temperature for 15-20 minutes. The
669 mixture was added dropwise to different areas of the well. Plates were incubated at 37°C,
670 5% CO2; 48hrs later, the virus-containing media was collected and filtered with a 0.45µm
671 low protein-binding filter. HEK-Blue IL-18 cells (InvivoGen) were seeded into a 6-well
672 plate in 1 mL growth media (DMEM with 10% (v/v) FBS, 100 units/mL penicillin, and 0.1
673 mg/mL streptomycin) and 1 mL virus-containing media. Cells were incubated at 37°C, 5%
674 CO2 for two days before the media was changed.
675
676 *Reporter cell stimulation and reading*. Purified IgG titrations and 2 nM IL-33 were mixed
677 in 50 µL assay media (DMEM with 10% (v/v) FBS, 100 units/mL penicillin, and 0.1 mg/mL
678 streptomycin) and incubated with shaking for 1 hour at room temperature. Approximately
679 50,000 IL-33 reporter cells in 50 µL assay media were added to wells of a sterile tissue
680 culture grade flat-bottom 96-well plate. IgG-IL-33 mixtures were added to respective wells
681 (1 nM IL-33 final concentration). Plates were incubated at 37°C, 5% CO2 for 20 hours,

682 then 20 μL media from each well was added to 180 μL room temperature QUANTI-Blue
683 Solution (InvivoGen) in a separate flat-bottom 96-well plate and incubated at 37°C for 3
684 hours. Absorbance at 655 nm was measured in a Synergy HTX Multi-Mode Microplate
685 Reader (BioTek). Percent max signal was calculated based on signal generated by IL-33
686 in the absence of any serum.
687
688 **ROC analysis of REAP score performance.**
689 Orthogonal validation data for the receiver operator curve (ROC) analysis was obtained
690 by ELISA, LIPS, or clinical autoantibody tests. For ELISA and LIPS, valid reactivities were
691 defined as those 3 standard deviations above the healthy donor average for a given
692 protein in each assay. ROC analysis was performed using 247 test pairs across 25
693 different proteins. A full list of ROC inputs can be found in **Supplementary Data 1**.
694
695 **Patient Samples**
696 *SLE patients.* Collection of SLE patient blood samples was approved by the Yale Human
697 Research Protection Program Institutional Review Boards (protocol ID 1602017276). All
698 patients met the 2012 SLICC classification criteria for SLE[63]. Clinical information was
699 gathered via retrospective EMR review. Informed consent was obtained from all patients.
700
701 *APECED patients.* Collection of APECED patient blood samples was performed under a
702 NIAID IRB-approved prospective natural history study (11-I-0187, NCT01386437).
703 Patients underwent a comprehensive clinical evaluation at the NIH Clinical Center
704 including a detailed history and physical examination, laboratory and radiologic
705 evaluations and consultations by a multidisciplinary team of specialists including
706 infectious disease, immunology, genetics, endocrinology, gastroenterology, hepatology,
707 pulmonology, dermatology, dental, and ophthalmology, as previously described[64]. All
708 study participants provided written informed consent.
709
710 **Statistical analysis**.
711 Statistical details of experiments can be found in the figure legends. All REAP screens
712 and experimental assays were performed with technical replicates. Data analysis was

713 performed using R, Python, Excel, and GraphPad Prism. Unless otherwise specified,
714 adjustment for false discovery rate was performed using the Benjamini-Hochberg
715 procedure.
716
717 **Data Availability**
718 Data are available from the corresponding author upon reasonable request.
719
720 **Code Availability**
721 All code will be available at GitHub.
722
723 **Figure Legends**
724 **Figure 1: Yeast library and REAP development. a,** Simplified schematic of REAP.
725 Antibodies are incubated with a genetically-barcoded yeast library displaying members of
726 the exoproteome in 96-well microtiter plates. Antibody bound yeast are enriched by
727 magnetic column-based sorting and enrichment is quantified by next-generation
728 sequencing. **b,** Composition of proteins in the yeast library, categorized by broad protein
729 families. Abbreviations are as follows: immunoglobulin superfamily (IgSF), epidermal
730 growth factor (EGF), fibronectin (Fn), leucine-rich repeat (LRR), urokinase receptor
731 (UPAR), c-type lectin (CLEC), tetraspanin (TSPAN). The cytokine family consists of
732 proteins belonging to tumor necrosis factor, interferon, interleukin, and growth factor
733 protein families. **c & d,** Distribution of total protein frequencies (**c**) and unique yeast clones
734 per protein in the yeast library (**d**). Solid lines indicate the median of the distribution and
735 dotted lines indicate first and third quartiles.
736
737 **Figure 2: Validation of REAP.** A panel of nine monoclonal antibodies were screened
738 using REAP. **a,** Heatmap of results from REAP screen of nine monoclonal antibodies.
739 Only relevant monoclonal antibody targets (gene names) are displayed. **b,**
740 Representative sample from the screen. Monoclonal antibody target is highlighted in red
741 and labelled. Background subtraction was performed by subtracting the score of a
742 selection performed with beads and secondary alone. Scores below the average

743 background level are not shown. **c,** REAP screen performed using recombinant protein
744 in place of IgG.
745
746 **Figure 3: REAP screen of APECED patients.** A cohort of 77 APECED patients and 20
747 healthy controls were screened using REAP. **a,** Heatmap of REAP scores. Antigen
748 groups were manually categorized. **b,** Frequencies of positive reactivities (score ≥ healthy
749 donor average score plus 3 standard deviations) against 14 antigens based on REAP
750 and prior literature[18,43,47]. **c,** Violin plot of GIF REAP scores in APECED samples stratified
751 by intrinsic factor clinical autoantibody test results. **d,** EC50 of fitted REAP and ELISA
752 dose response curves for detection of autoantibodies against four proteins in one
753 APECED patient. See **supplementary figure 1e,f** for dose response curves. **e,** Violin
754 plot of the number of reactivities in APECED and control samples at a score cutoff of 3.
755 **f,** anti-GPHB5 and **g,** anti-PNLIP pan-IgG ELISAs conducted with serial dilutions of
756 serum. Error bars represent standard deviation. **h,** Heatmap of LCN1 and BPIFA1 REAP
757 scores in APECED samples stratified by pneumonitis positivity. Listed p-values represent
758 significance for the association between LCN1 or BPIFA1 REAP positivity and
759 pneumonitis. Significance in **c** and **e** was determined using a two-sided Mann-Whitney U
760 test. Significance in **h** was determined using a Fisher Exact Test, where LCN1 and
761 BPIFA1 positivity was defined by a REAP score ≥ 3. In all heatmaps in this figure, score
762 was artificially capped at 7 to aid visualization. In all violin plots in this figure, solid lines
763 represent the median and dotted lines represent the first or third quartile. ****P ≤ 0.0001
764
765 **Figure 4: REAP screen of SLE patients.** A cohort of 106 unique SLE patients spanning
766 155 samples and 20 healthy controls was screened using REAP. **a**, Heatmap of REAP
767 scores where each column is a unique patient. For patients with longitudinal samples, the
768 maximum REAP score for each given reactivity is shown. Antigen groups were manually
769 categorized. Patients are ordered from left to right by increasing SLEDAI score. White
770 stars symbolize detection of a therapeutic antibody. Score was artificially capped at 7 to
771 aid visualization. **b,** Violin plots of the number of reactivities in SLE samples stratified by
772 disease severity and control samples at a score cutoff of 3. Significance was determined
773 using a Kruskal-Wallis test followed by a Dunnett's test. **c,** Heatmap of false discovery

774 rate-adjusted p-values from two-sided Mann-Whitney U tests comparing REAP score
775 distributions for specific proteins between patients stratified by disease manifestations.
776 Only reactivities positive in at least 3 patients were tested. **d,** SLEDAI scores for SLE
777 patients stratified by reactivity against CCL8. **e,** SLEDAI scores for SLE patients positive
778 or negative by REAP score for reactivities against immunoregulatory antigens (defined in
779 **a**). **f,** anti-PD-L2 and **i,** anti-IL-33 pan-IgG ELISAs conducted with serial dilutions of SLE
780 or control serum. **g,** schematic and **h,** results of PD-L2 blocking assay conducted with
781 serial dilutions of serum from a control and the SLE patient in **f**. **j,** schematic and **k,** results
782 of IL-33 neutralization assay conducted with serial dilutions of IgG from a control and the
783 SLE patient in **i**. Significance in **d** and **e** was determined using a two-sided Mann-Whitney
784 U test. All error bars in this figure represent standard deviation. For all analyses in this
785 figure, positive reactivities were defined as those with REAP score ≥ 3. *P ≤ 0.05, **P ≤
786 0.01.
787
788 **Table 1 | Orthogonal validation of SLE autoantibody reactivities identified in**
789 **REAP.**
790
791 **Supplementary Figure 1 | Exoproteome yeast display library properties. a,** Flowchart
792 of steps in identification and annotation of extracellular or secreted proteins for inclusion
793 in the library. **b,** Pie chart of all extracellular or secreted proteins identified in **a**. Proteins
794 were not attempted if they had an ectodomain less than 50 amino acids or less than 600
795 amino acids. **c,** Percent of proteins displayed in each protein family included in the library.
796 The dotted line represents the aggregate display level in the library. Abbreviations are as
797 follows: immunoglobulin superfamily (IgSF), epidermal growth factor (EGF), fibronectin
798 (Fn), leucine-rich repeat (LRR), urokinase receptor (UPAR), c-type lectin (CLEC),
799 tetraspanin (TSPAN). The cytokine family consists of proteins belonging to tumor necrosis
800 factor, interferon, interleukin, and growth factor protein families. **d,** Box plot of Log_2[fold
801 enrichment] R^2 coefficient of determination values between technical replicates of
802 APECED patients screened in **figure 2**. **e & f,** REAP (**e**) versus ELISA (**f**) dose-response
803 curve comparison for APECED autoantibodies against four proteins. REAP data is from
804 a screen conducted using varying concentrations of AIRE.19 IgG. Curves were fit using

805 a sigmoidal 4 parameter logistic curve. For REAP, curves were fit based on Log_2[fold
806 enrichment]. For ELISA, curves were fit based on optical density at 450 nm. Error bars
807 represent standard error of the mean. **g,** Comparison of autoantibody detection
808 frequencies in APECED patient cohorts by REAP, LIPS[18], ProtoArray[18], and PhIP-Seq[21].
809 Frequencies are listed as a percentage inside each circle. Size and color of circles are
810 proportional to detection frequency. For REAP, detection frequency was calculated as in
811 **figure 2b**. For LIPS and ProtoArray, detection frequencies were provided in the
812 corresponding publication. For PhIP-Seq, detection frequency was calculated based on
813 figures in the corresponding publication. For reactivities labelled n.d., either data was not
814 publicly available or the autoantibody was not tested for in the corresponding assay.
815
816 **Supplementary Figure 2 | APECED and SLE reactivity distributions. a,** Violin plots of
817 the number of reactivities in APECED and control samples at a score cutoff of 1 or 2. **b,**
818 Mean number of reactivities in APECED and control samples at various score cutoffs,
819 along with indicators of significance. **c,** Violin plots of the number of reactivities in SLE
820 samples stratified by disease severity and control samples at a score cutoff of 1 or 2. **d,**
821 Mean number of reactivities in SLE samples stratified by disease severity and control
822 samples at various score cutoffs. Comparisons were made between each disease
823 severity group and the control group. Significance in **a** and **b** was calculated using a two-
824 sided Mann-Whitney U test. Significance in **c** and **d** was determined using a Kruskal-
825 Wallis test followed by a Dunnett's test.
826
827 **Supplementary Figure 3 | REAP validation and ROC analysis. a-l,** Single-point
828 ELISAs or LIPS conducted with SLE, APECED, or control serum to detect autoantibodies
829 against ACVR2B (**a**), CCL8 (**b**), CSPG5 (**c**), CXCL3 (**d**), Fas (**e**), IL-4 (**f**), IL-6 (**g**), IL-16
830 (**h**), IL-22 (**i**), IFN-α8 (**j**), IFN-α7 (**k**), and IFNL2 (**l**). Serum dilutions are listed in the title of
831 each plot. **m-r,** ELISAs or LIPS conducted with serial dilutions of SLE, APECED, or control
832 serum to detect autoantibodies against BPIFA2 (**m**), EPYC (**n**), IER3 (**o**), IL18RAP (**p**),
833 LILRB4 (**q**), and VEGF-B (**r**). Dotted lines in **a-l** represent the control average + 3 standard
834 deviations. **s,** Receiver operating characteristic curve of the ability of REAP score to
835 predict validation of a REAP reactivity in an orthogonal assay. A full description of this

836 analysis can be found in the materials and methods section. **t,** Anti-epiphycan IgG
837 subclass specific ELISA conducted with serial dilutions of serum from the SLE patient
838 with highest titers in **n**. **u,** Anti-IL-18RAcP subclass specific ELISA conducted with serial
839 dilutions of serum from the SLE patient in **p**. **v,** Anti-PD-L2 IgG subclass specific ELISAs
840 conducted with serial dilutions of serum from the SLE patient in **figure 3f**. All error bars
841 in this figure all represent standard deviation. All curves in this figure were fit using a
842 sigmoidal 4 parameter logistic curve.
843
844 **Supplementary Table 1 | List of protein antigens included in library**
845
846 **Supplementary Table 2 | APECED patient demographics and clinical**
847 **characteristics.**
848
849 **Supplementary Table 3 | SLE patient and control demographics and clinical**
850 **characteristics.**
851
852 **Supplementary Data 1 | Receiver operating characteristic analysis inputs**
853
854 **References**

855 1. Ludwig, R. J. *et al.* Mechanisms of Autoantibody-Induced Pathology. *Front.*
856 *Immunol.* **8**, 603 (2017).
857 2. Kazarian, M. & Laird-Offringa, I. A. Small-cell lung cancer-associated
858 autoantibodies: potential applications to cancer diagnosis, early detection, and
859 therapy. *Mol. Cancer* **10**, 33 (2011).
860 3. Leslie, R. D., Palmer, J., Schloot, N. C. & Lernmark, A. Diabetes at the crossroads:
861 relevance of disease classification to pathophysiology and treatment. *Diabetologia*
862 **59**, 13–20 (2016).
863 4. Menconi, F., Marcocci, C. & Marinò, M. Diagnosis and classification of Graves'
864 disease. *Autoimmun. Rev.* **13**, 398–402 (2014).
865 5. Meier, L. A. & Binstadt, B. A. The Contribution of Autoantibodies to Inflammatory
866 Cardiovascular Pathology. *Front. Immunol.* **9**, 911 (2018).

867 6. Ercolini, A. M. & Miller, S. D. The role of infections in autoimmune disease. *Clin.*
868 *Exp. Immunol.* **155**, 1–15 (2009).
869 7. De Virgilio, A. *et al.* Parkinson's disease: Autoimmunity and neuroinflammation.
870 *Autoimmun. Rev.* **15**, 1005–1011 (2016).
871 8. Britschgi, M. *et al.* Neuroprotective natural antibodies to assemblies of
872 amyloidogenic peptides decrease with normal aging and advancing Alzheimer's
873 disease. *Proc. Natl. Acad. Sci. U. S. A.* **106**, 12145–12150 (2009).
874 9. Cappellano, G. *et al.* Anti-cytokine autoantibodies in autoimmune diseases. *Am. J.*
875 *Clin. Exp. Immunol.* **1**, 136–146 (2012).
876 10. Watanabe, M., Uchida, K., Nakagaki, K., Trapnell, B. C. & Nakata, K. High avidity
877 cytokine autoantibodies in health and disease: pathogenesis and mechanisms.
878 *Cytokine Growth Factor Rev.* **21**, 263–273 (2010).
879 11. Tabuchi, Y. *et al.* Protective effect of naturally occurring anti-HER2 autoantibodies
880 on breast cancer. *Breast Cancer Res. Treat.* **157**, 55–63 (2016).
881 12. Gillissen, M. A. *et al.* Patient-derived antibody recognizes a unique CD43 epitope
882 expressed on all AML and has antileukemia activity in mice. *Blood Adv* **1**, 1551–
883 1564 (2017).
884 13. von Mensdorff-Pouilly, S. *et al.* Survival in early breast cancer patients is favorably
885 influenced by a natural humoral immune response to polymorphic epithelial mucin.
886 *J. Clin. Oncol.* **18**, 574–583 (2000).
887 14. Naparstek, Y. & Plotz, P. H. The Role of Autoantibodies in Autoimmune Disease.
888 *Annual Review of Immunology* **11**, 79–104 (1993).
889 15. Larman, H. B. *et al.* Autoantigen discovery with a synthetic human peptidome. *Nat.*
890 *Biotechnol.* **29**, 535–541 (2011).
891 16. Larman, H. B. *et al.* PhIP-Seq characterization of autoantibodies from patients with
892 multiple sclerosis, type 1 diabetes and rheumatoid arthritis. *J. Autoimmun.* **43**, 1–9
893 (2013).
894 17. Benjamin Larman, H. *et al.* Cytosolic 5′-nucleotidase 1A autoimmunity in sporadic
895 inclusion body myositis: cN1A Autoimmunity in IBM. *Ann. Neurol.* **73**, 408–418
896 (2013).
897 18. Meyer, S. *et al.* AIRE-Deficient Patients Harbor Unique High-Affinity Disease-

898 Ameliorating Autoantibodies. *Cell* **166**, 582–595 (2016).
899 19. Landegren, N. *et al.* Proteome-wide survey of the autoimmune target repertoire in
900 autoimmune polyendocrine syndrome type 1. *Sci. Rep.* **6**, 20104 (2016).
901 20. Fishman, D. *et al.* Autoantibody Repertoire in APECED Patients Targets Two
902 Distinct Subgroups of Proteins. *Front. Immunol.* **8**, 976 (2017).
903 21. Vazquez, S. E. *et al.* Identification of novel, clinically correlated autoantigens in the
904 monogenic autoimmune syndrome APS1 by proteome-wide PhIP-Seq. *Elife* **9**,
905 (2020).
906 22. Kamath, K. *et al.* Antibody epitope repertoire analysis enables rapid antigen
907 discovery and multiplex serology. *Sci. Rep.* **10**, 5294 (2020).
908 23. Chen, W. S. *et al.* Autoantibody Landscape in Patients with Advanced Prostate
909 Cancer. *Clin. Cancer Res.* **26**, 6204–6214 (2020).
910 24. Laver, W. G., Air, G. M., Webster, R. G. & Smith-Gill, S. J. Epitopes on protein
911 antigens: misconceptions and realities. *Cell* **61**, 553–556 (1990).
912 25. Gai, S. A. & Wittrup, K. D. Yeast surface display for protein engineering and
913 characterization. *Curr. Opin. Struct. Biol.* **17**, 467–473 (2007).
914 26. Weiskopf, K. *et al.* Engineered SIRPα variants as immunotherapeutic adjuvants to
915 anticancer antibodies. *Science* **341**, 88–91 (2013).
916 27. Warren, J. T. *et al.* Manipulation of receptor oligomerization as a strategy to inhibit
917 signaling by TNF superfamily members. *Sci. Signal.* **7**, ra80 (2014).
918 28. Schweickhardt, R. L., Jiang, X., Garone, L. M. & Brondyk, W. H. Structure-
919 Expression Relationship of Tumor Necrosis Factor Receptor Mutants That Increase
920 Expression*. *J. Biol. Chem.* **278**, 28961–28967 (2003).
921 29. Jin, M. *et al.* Directed evolution to probe protein allostery and integrin I domains of
922 200,000-fold higher affinity. *Proc. Natl. Acad. Sci. U. S. A.* **103**, 5758–5763 (2006).
923 30. Chen, T. F., de Picciotto, S., Hackel, B. J. & Wittrup, K. D. Engineering fibronectin-
924 based binding proteins by yeast surface display. *Methods Enzymol.* **523**, 303–326
925 (2013).
926 31. Xu, G., Tasumi, S. & Pancer, Z. Yeast surface display of lamprey variable
927 lymphocyte receptors. *Methods Mol. Biol.* **748**, 21–33 (2011).
928 32. Chao, G., Cochran, J. R. & Wittrup, K. D. Fine epitope mapping of anti-epidermal

929 growth factor receptor antibodies through random mutagenesis and yeast surface
930 display. *J. Mol. Biol.* **342**, 539–550 (2004).
931 33. Jeong, M.-Y., Rutter, J. & Chou, D. H.-C. Display of Single-Chain Insulin-like
932 Peptides on a Yeast Surface. *Biochemistry* **58**, 182–188 (2019).
933 34. Levin, A. M. *et al.* Exploiting a natural conformational switch to engineer an
934 interleukin-2 'superkine'. *Nature* **484**, 529–533 (2012).
935 35. Zhou, T. *et al.* IL-18BP is a secreted immune checkpoint and barrier to IL-18
936 immunotherapy. *Nature* **583**, 609–614 (2020).
937 36. Ho, C. C. M. *et al.* Decoupling the Functional Pleiotropy of Stem Cell Factor by
938 Tuning c-Kit Signaling. *Cell* **168**, 1041–1052.e18 (2017).
939 37. Boder, E. T., Bill, J. R., Nields, A. W., Marrack, P. C. & Kappler, J. W. Yeast
940 surface display of a noncovalent MHC class II heterodimer complexed with
941 antigenic peptide. *Biotechnol. Bioeng.* **92**, 485–491 (2005).
942 38. Birnbaum, M. E. *et al.* Deconstructing the peptide-MHC specificity of T cell
943 recognition. *Cell* **157**, 1073–1087 (2014).
944 39. Kieke, M. C. *et al.* Selection of functional T cell receptor mutants from a yeast
945 surface-display library. *Proc. Natl. Acad. Sci. U. S. A.* **96**, 5651–5656 (1999).
946 40. Rhiel, L. *et al.* REAL-Select: full-length antibody display and library screening by
947 surface capture on yeast cells. *PLoS One* **9**, e114887 (2014).
948 41. Boder, E. T. & Wittrup, K. D. Yeast surface display for screening combinatorial
949 polypeptide libraries. *Nat. Biotechnol.* **15**, 553–557 (1997).
950 42. Constantine, G. M. & Lionakis, M. S. Lessons from primary immunodeficiencies:
951 Autoimmune regulator and autoimmune polyendocrinopathy-candidiasis-
952 ectodermal dystrophy. *Immunol. Rev.* **287**, 103–120 (2019).
953 43. Meager, A. *et al.* Anti-interferon autoantibodies in autoimmune polyendocrinopathy
954 syndrome type 1. *PLoS Med.* **3**, e289 (2006).
955 44. Wolff, A. S. B. *et al.* Autoimmune polyendocrine syndrome type 1 in Norway:
956 phenotypic variation, autoantibodies, and novel mutations in the autoimmune
957 regulator gene. *J. Clin. Endocrinol. Metab.* **92**, 595–603 (2007).
958 45. Meloni, A. *et al.* Autoantibodies against type I interferons as an additional
959 diagnostic criterion for autoimmune polyendocrine syndrome type I. *J. Clin.*

960 *Endocrinol. Metab.* **93**, 4389–4397 (2008).
961 46. Puel, A. *et al.* Autoantibodies against IL-17A, IL-17F, and IL-22 in patients with
962 chronic mucocutaneous candidiasis and autoimmune polyendocrine syndrome type
963 I. *J. Exp. Med.* **207**, 291–297 (2010).
964 47. Kisand, K. *et al.* Chronic mucocutaneous candidiasis in APECED or thymoma
965 patients correlates with autoimmunity to Th17-associated cytokines. *J. Exp. Med.*
966 **207**, 299–308 (2010).
967 48. Burbelo, P. D. *et al.* Profiling Autoantibodies against Salivary Proteins in Sicca
968 Conditions. *J. Dent. Res.* **98**, 772–778 (2019).
969 49. St-Pierre, C., Trofimov, A., Brochu, S., Lemieux, S. & Perreault, C. Differential
970 Features of AIRE-Induced and AIRE-Independent Promiscuous Gene Expression
971 in Thymic Epithelial Cells. *J. Immunol.* **195**, 498–506 (2015).
972 50. Ferré, E. M. N. *et al.* Lymphocyte-driven regional immunopathology in pneumonitis
973 caused by impaired central immune tolerance. *Sci. Transl. Med.* **11**, (2019).
974 51. Lowe, M. E. Structure and Function of Pancreatic Lipase and Colipase. *Annual*
975 *Reviews of Immunology* **17**, 141–158 (1997).
976 52. Tsokos, G. C., Lo, M. S., Costa Reis, P. & Sullivan, K. E. New insights into the
977 immunopathogenesis of systemic lupus erythematosus. *Nat. Rev. Rheumatol.* **12**,
978 716–730 (2016).
979 53. Pisetsky, D. S. & Lipsky, P. E. New insights into the role of antinuclear antibodies in
980 systemic lupus erythematosus. *Nat. Rev. Rheumatol.* **16**, 565–579 (2020).
981 54. Bombardier, C., Gladman, D. D., Urowitz, M. B., Caron, D. & Chang, C. H.
982 Derivation of the SLEDAI. A disease activity index for lupus patients. The
983 Committee on Prognosis Studies in SLE. *Arthritis Rheum.* **35**, 630–640 (1992).
984 55. Yang, Z., Liang, Y., Xi, W., Li, C. & Zhong, R. Association of increased serum IL-33
985 levels with clinical and laboratory characteristics of systemic lupus erythematosus
986 in Chinese population. *Clin. Exp. Med.* **11**, 75–80 (2011).
987 56. Guo, J. *et al.* The association of novel IL-33 polymorphisms with sIL-33 and risk of
988 systemic lupus erythematosus. *Mol. Immunol.* **77**, 1–7 (2016).
989 57. Rose, W. A., 2nd *et al.* Interleukin-33 Contributes Toward Loss of Tolerance by
990 Promoting B-Cell-Activating Factor of the Tumor-Necrosis-Factor Family (BAFF)-

991 Dependent Autoantibody Production. *Front. Immunol.* **9**, 2871 (2018).
992 58. Li, P., Lin, W. & Zheng, X. IL-33 neutralization suppresses lupus disease in lupus-
993 prone mice. *Inflammation* **37**, 824–832 (2014).
994 59. Herscovics, A. & Orlean, P. Glycoprotein biosynthesis in yeast. *FASEB J.* **7**, 540–
995 550 (1993).
996 60. Hamilton, S. R. & Gerngross, T. U. Glycosylation engineering in yeast: the advent
997 of fully humanized yeast. *Curr. Opin. Biotechnol.* **18**, 387–392 (2007).
998 61. Picelli, S. *et al.* Tn5 transposase and tagmentation procedures for massively scaled
999 sequencing projects. *Genome Res.* **24**, 2033–2040 (2014).
1000 62. Robinson, M. D., McCarthy, D. J. & Smyth, G. K. edgeR: a Bioconductor package
1001 for differential expression analysis of digital gene expression data. *Bioinformatics*
1002 **26**, 139–140 (2010).
1003 63. Petri, M. *et al.* Derivation and validation of the Systemic Lupus International
1004 Collaborating Clinics classification criteria for systemic lupus erythematosus.
1005 *Arthritis Rheum.* **64**, 2677–2686 (2012).
1006 64. Ferre, E. M. N. *et al.* Redefined clinical features and diagnostic criteria in
1007 autoimmune polyendocrinopathy-candidiasis-ectodermal dystrophy. *JCI Insight* **1**,
1008 (2016).
1009

1010 **Acknowledgements**

1011 The authors gratefully acknowledge all members of the Ring Laboratory and Daniela
1012 Deny for helpful advice and technical assistance. The authors also thank the Yale Section
1013 of Rheumatology, Allergy & Imunology for providing systemic lupus erythematosus (SLE)
1014 samples from its repository as well as the members of the Yale Rheumatology Clinical
1015 and Translational Research Laboratory, Shannon Teaw BS and Michelle Cheng BA for
1016 aliquoting SLE patient sera. This work was supported by gifts from the Mathers Family
1017 Foundation, the Colton Foundation, the Ludwig Family Foundation, and a supplement to
1018 the Yale Cancer Center Support Grant 3P30CA016359-40S4. A.M.R. is additionally
1019 supported by an NIH Director's Early Independence Award (DP5OD023088), a Pew-
1020 Stewart Award, and the Robert T. McCluskey Foundation. This work was supported by

the Division of Intramural Research of the National Institute of Allergy and Infectious Diseases, NIH.

Author Contributions

E.Y.W., Y.D., C.E.R., F.L., and Y.Y. performed experiments. M.X.D. provided lupus patient samples and clinical annotations. M.M.S., E.M.N.F., and M.S.L. provided APECED patient samples and clinical annotations. E.Y.W., Y.D., E.M., M.S.L., and A.M.R. analyzed data, M.H., M.S.L., and A.M.R. provided project supervision. E.Y.W. and A.M.R. wrote the paper.

Competing Interests

E.Y.W., Y.D., C.E.R., and A.M.R. are inventors of a patent describing the REAP technology and A.M.R. is the founder of Seranova Bio.

Figure 1

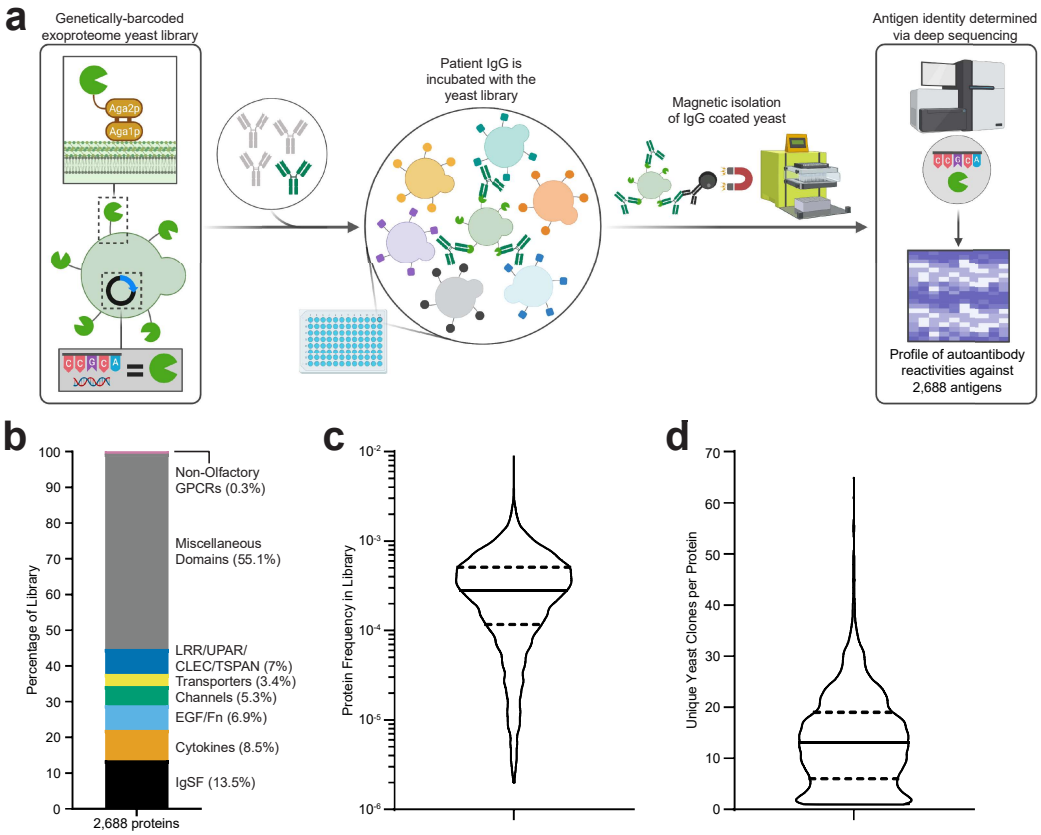
a
Genetically-barcoded exoproteome yeast library
Aga2p
Aga1p
Patient IgG is incubated with the yeast library
Magnetic isolation of IgG coated yeast
Antigen identity determined via deep sequencing
Profile of autoantibody reactivities against 2,688 antigens
b
Percentage of Library
Non-Olfactory GPCRs (0.3%)
Miscellaneous Domains (55.1%)
LRR/UPAR/ CLEC/TSPAN (7%)
Transporters (3.4%)
Channels (5.3%)
EGF/Fn (6.9%)
Cytokines (8.5%)
IgSF (13.5%)
2,688 proteins
c
Protein Frequency in Library
d
Unique Yeast Clones per Protein

Figure 2

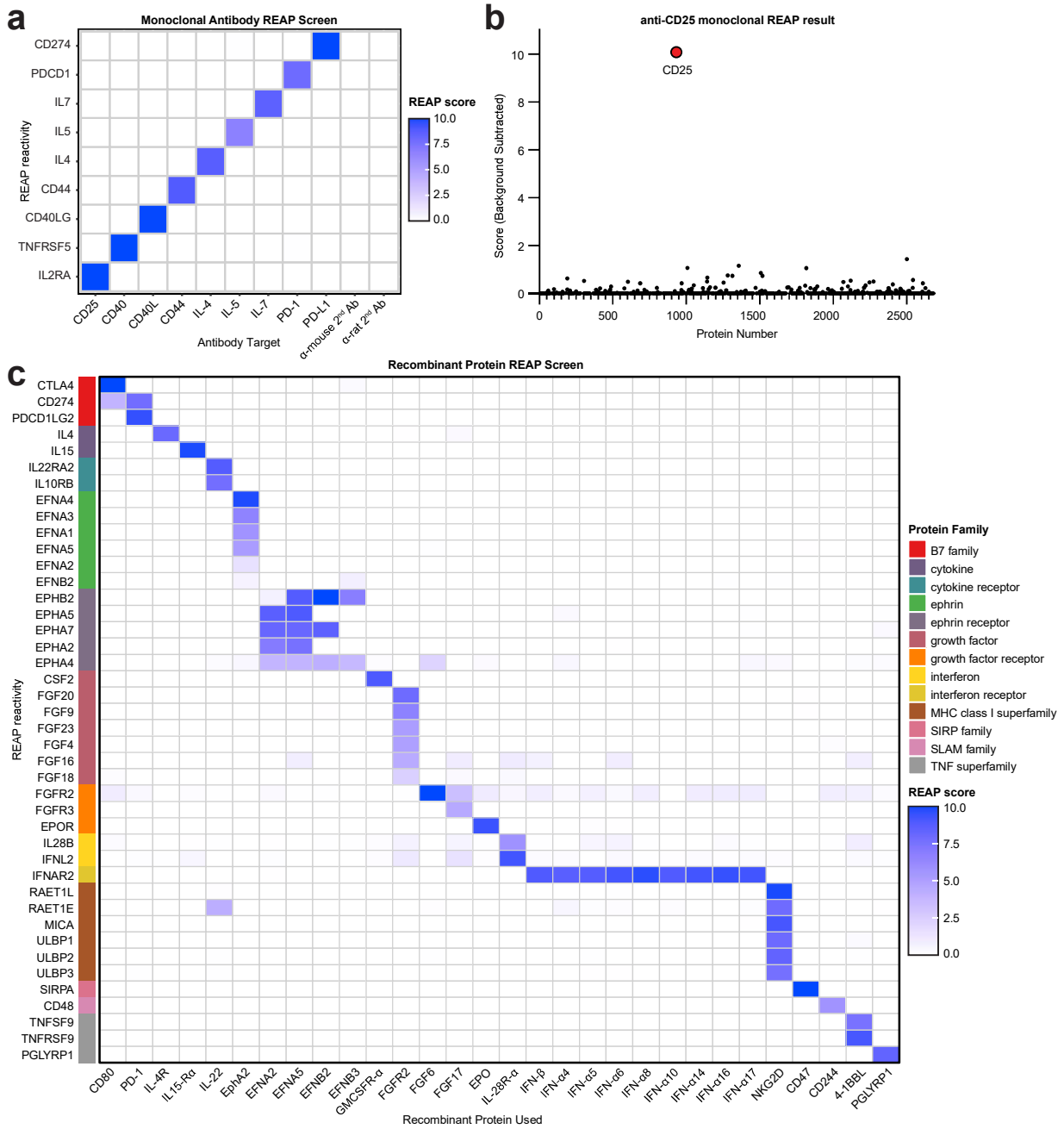
a
Monoclonal Antibody REAP Screen
REAP reactivity
CD274
PDCD1
IL7
IL5
IL4
CD44
CD40LG
TNFRSF5
IL2RA
CD25
CD40
CD40L
CD44
IL-4
IL-5
IL-7
PD-1
PD-L1
α-mouse 2nd Ab
α-rat 2nd Ab
Antibody Target
REAP score
10.0
7.5
5.0
2.5
0.0
b
anti-CD25 monoclonal REAP result
CD25
Score (Background Subtracted)
Protein Number
c
Recombinant Protein REAP Screen
REAP reactivity
CTLA4
CD274
PDCD1LG2
IL4
IL15
IL22RA2
IL10RB
EFNA4
EFNA3
EFNA1
EFNA5
EFNA2
EFNB2
EPHB2
EPHA5
EPHA7
EPHA2
EPHA4
CSF2
FGF20
FGF9
FGF23
FGF4
FGF16
FGF18
FGFR2
FGFR3
EPOR
IL28B
IFNL2
IFNAR2
RAET1L
RAET1E
MICA
ULBP1
ULBP2
ULBP3
SIRPA
CD48
TNFSF9
TNFRSF9
PGLYRP1
CD80
PD-1
IL-4R
IL15-Rα
IL-22
EphA2
EFNA2
EFNA5
EFNB2
EFNB3
GMCSFR-α
FGFR2
FGF6
FGF17
EPO
IL-28R-α
IFN-β
IFN-α4
IFN-α5
IFN-α6
IFN-α8
IFN-α10
IFN-α14
IFN-α16
IFN-α17
NKG2D
CD47
CD244
4-1BBL
PGLYRP1
Recombinant Protein Used
Protein Family
B7 family
cytokine
cytokine receptor
ephrin
ephrin receptor
growth factor
growth factor receptor
interferon
interferon receptor
MHC class I superfamily
SIRP family
SLAM family
TNF superfamily
REAP score
10.0
7.5
5.0
2.5
0.0

Figure 3

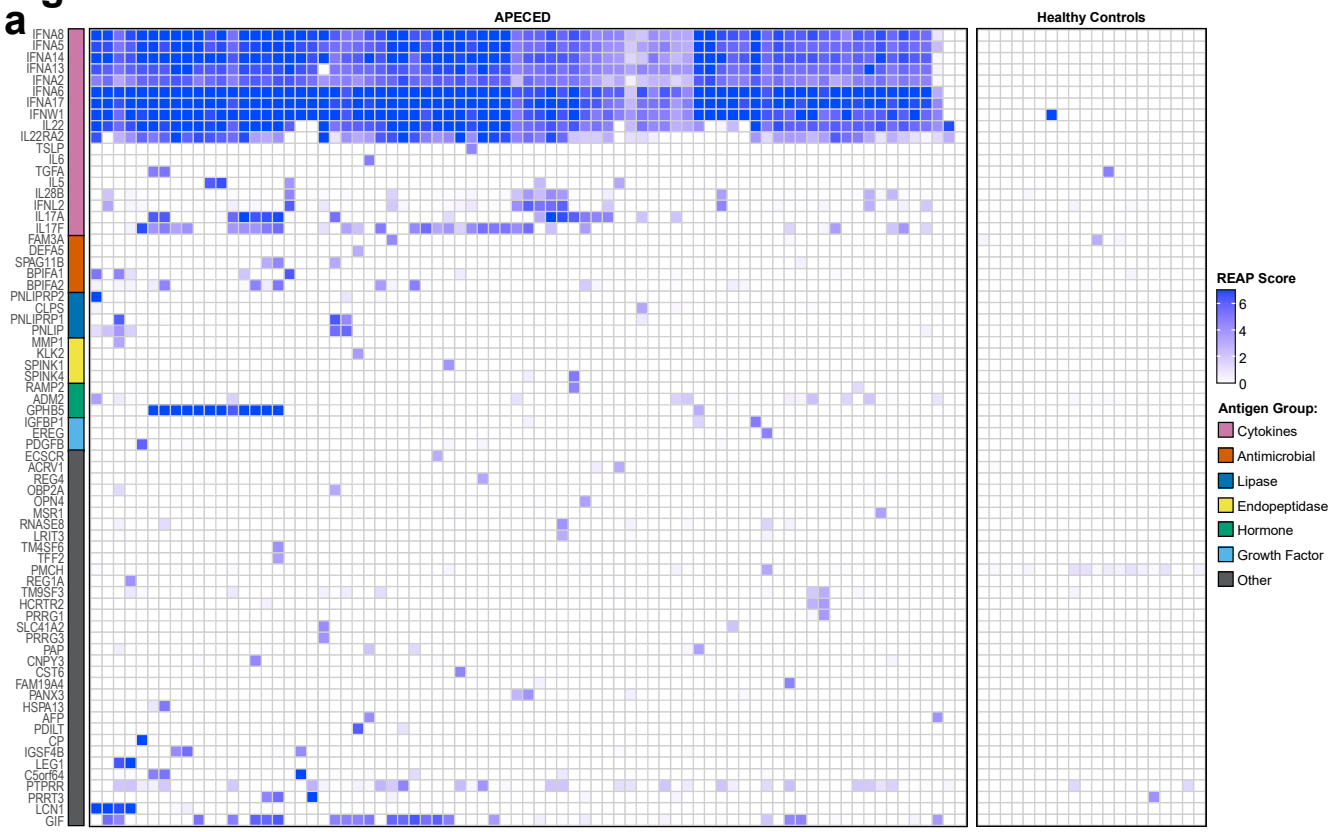

b

Antigen	REAP Frequency	Reported Frequency
IFN-α2	97.4	100[18,43]
IFN-α5	97.4	100[18]
IFN-α6	98.7	100[18]
IFN-α8	97.4	100[18]
IFN-α13	98.7	100[18]
IFN-α14	97.4	100[18]
IFN-α17	97.4	100[18]
IFN-ω	83.1	100[18,43]
IFN-λ2	22.1	28[18]
IFN-λ3	19.5	28[18]
IL-22	97.4	91[47], 94[18]
IL-17A	27.27	35[18], 41[47]
IL-17F	58.4	70[18], 75[47]
IL-5	9.1	16[18]

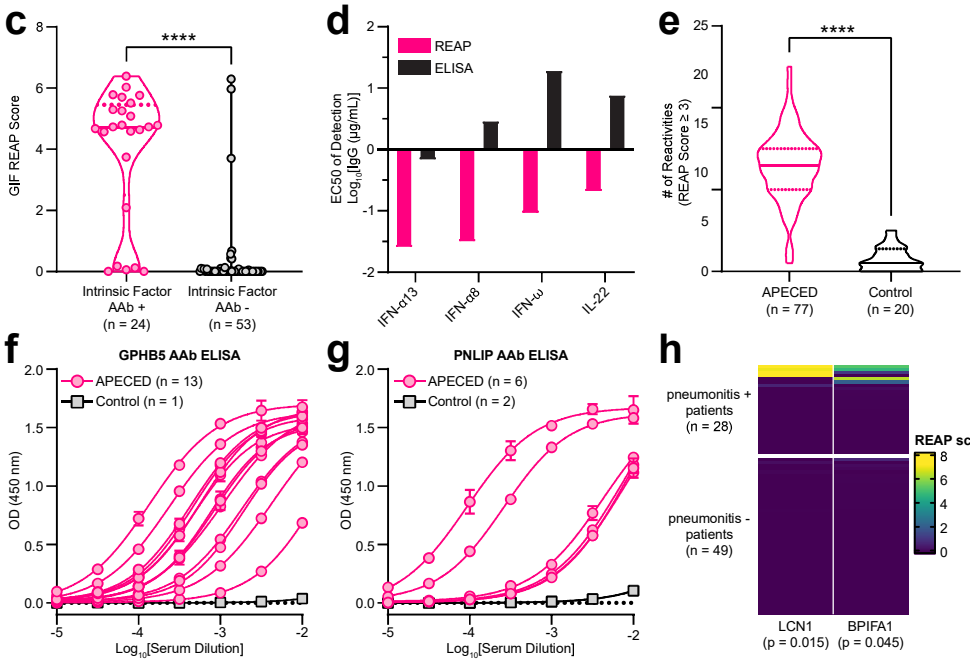

Figure 4

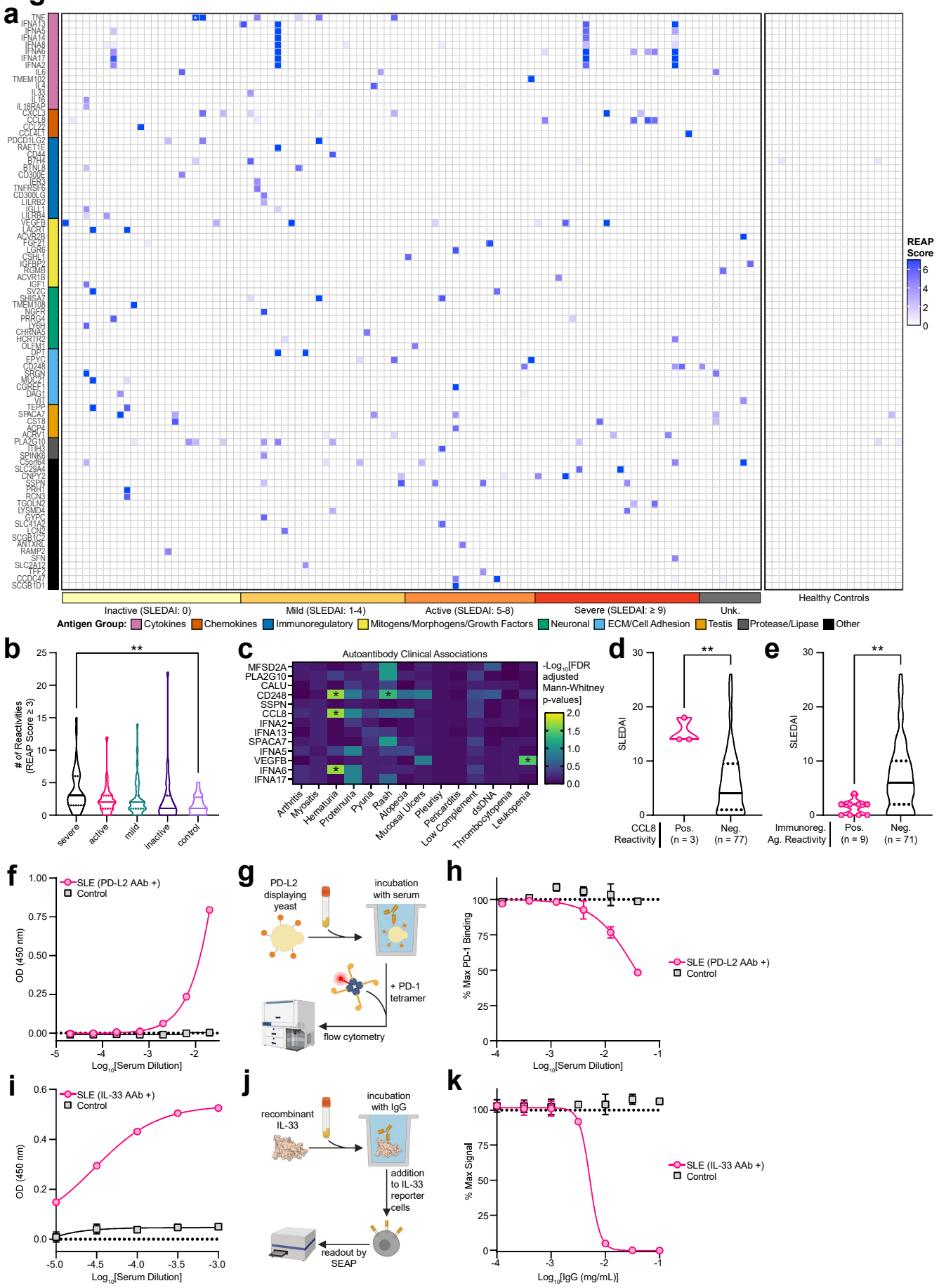
a
REAP Score
Healthy Controls
Inactive (SLEDAI: 0)
Mild (SLEDAI: 1-4)
Active (SLEDAI: 5-8)
Severe (SLEDAI: ≥ 9)
Unk.
Antigen Group: Cytokines Chemokines Immunoregulatory Mitogens/Morphogens/Growth Factors Neuronal ECM/Cell Adhesion Testis Protease/Lipase Other
b
# of Reactivities (REAP Score ≥ 3)
severe
active
mild
inactive
control
c
Autoantibody Clinical Associations
-Log10[FDR adjusted Mann-Whitney p-values]
MFSD2A
PLA2G10
CALU
CD248
SSPN
CCL8
IFNA2
IFNA13
SPACA7
IFNA5
VEGFB
IFNA6
IFNA17
Arthritis
Myositis
Hematuria
Proteinuria
Pyuria
Rash
Alopecia
Mucosal Ulcers
Pleurisy
Pericarditis
Low Complement
dsDNA
Thrombocytopenia
Leukopenia
d
SLEDAI
CCL8 Reactivity
Pos. (n = 3)
Neg. (n = 77)
e
SLEDAI
Immunoreg. Ag. Reactivity
Pos. (n = 9)
Neg. (n = 71)
f
SLE (PD-L2 AAb +)
Control
OD (450 nm)
Log10[Serum Dilution]
g
PD-L2 displaying yeast
incubation with serum
+ PD-1 tetramer
flow cytometry
h
% Max PD-1 Binding
Log10[Serum Dilution]
SLE (PD-L2 AAb +)
Control
i
SLE (IL-33 AAb +)
Control
OD (450 nm)
Log10[Serum Dilution]
j
recombinant IL-33
incubation with IgG
addition to IL-33 reporter cells
readout by SEAP
k
% Max Signal
Log10[IgG (mg/mL)]
SLE (IL-33 AAb +)
Control

Table 1

Table 1 | Orthogonal validation of SLE autoantibody reactivities identified in REAP.

Antigen	# Candidate Samples Tested	REAP Score Range	# Validated by ELISA or LIPS
VEGF-B	10	1.67 - 8.88	10
IFN-α17	8	1.85 - 10.33	8
IFN-α8	7	1.13 - 8.92	4
FAS	6	1.73 - 4.95	4
EPYC	4	4.93 - 9.46	4
CSPG5	6	1.64 - 5.92	3
IL-6	3	3.60 - 7.82	3
PD-L2	4	2.43 - 9.69	2
IL-4	2	5.78 - 6.09	2
CCL8	4	4.59 - 6.44	1
IL-33	1	3.88	1
IL-18Rβ	1	3.3	1
IL-16	1	4.03	1
LILRB4	1	3.85	1
ACVR2B	1	8.56	1
IER3	1	4.23	1
IFNL2	6	3.27 - 7.74	0
NGFR	4	3.40 - 6.73	0
RGMB	4	4.15 - 5.49	0
CD44	1	6.34	0
RAET1E	1	7.6	0

Supplementary Figure 1

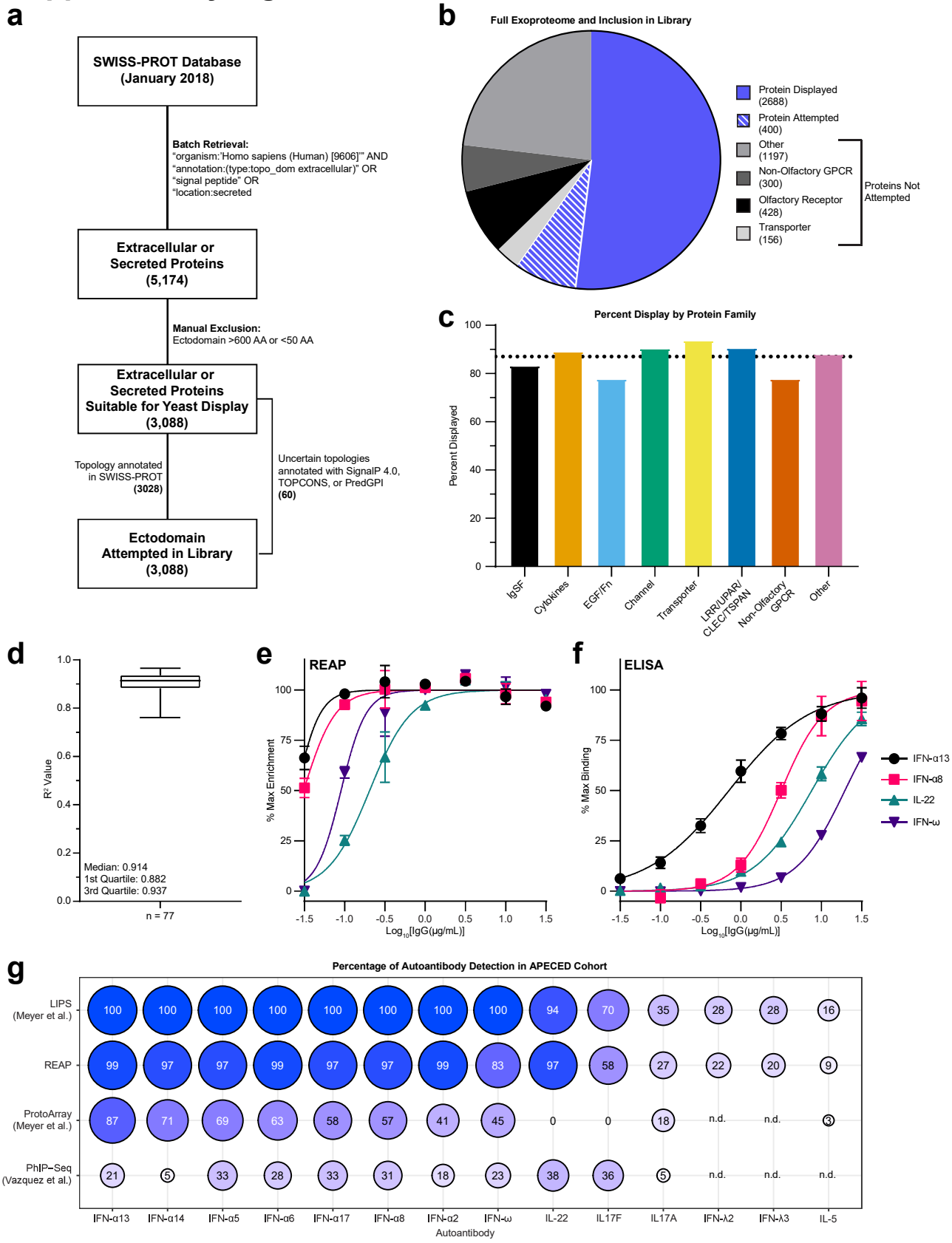

Supplementary Figure 2

a

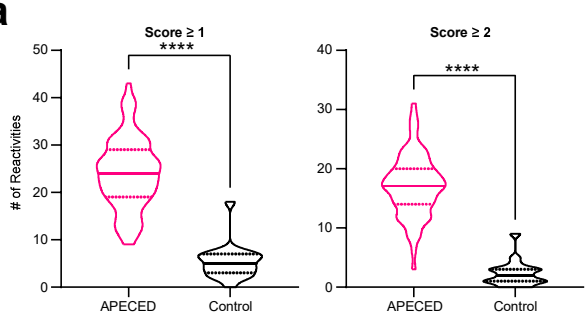

b

Average # of Reactivities per Sample

	APECED (n = 77)	control (n = 20)
score ≥ 1	24.03 ****	5.30
score ≥ 2	17.12 ****	2.25
score ≥ 3	12.95 ****	1.50
score ≥ 4	10.69 ****	1.25
score ≥ 5	8.73 ****	0.75
score ≥ 6	6.29 ****	0.40

c

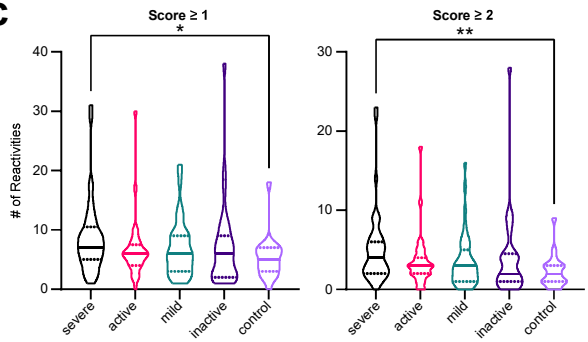

d

Average # of Reactivities per Sample

	severe (n = 45)	active (n = 33)	mild (n = 43)	inactive (n = 34)	control (n = 20)
score ≥ 1	8.67 *	6.67	6.98	6.97	5.30
score ≥ 2	5.13 **	3.52	3.47	3.79	2.25
score ≥ 3	3.64 **	2.30	2.51	2.53	1.50
score ≥ 4	2.69	1.67	1.72	1.74	1.25
score ≥ 5	1.91	0.91	1.35	1.06	0.75
score ≥ 6	1.13	0.45	0.95	0.79	0.40

Supplementary Figure 3

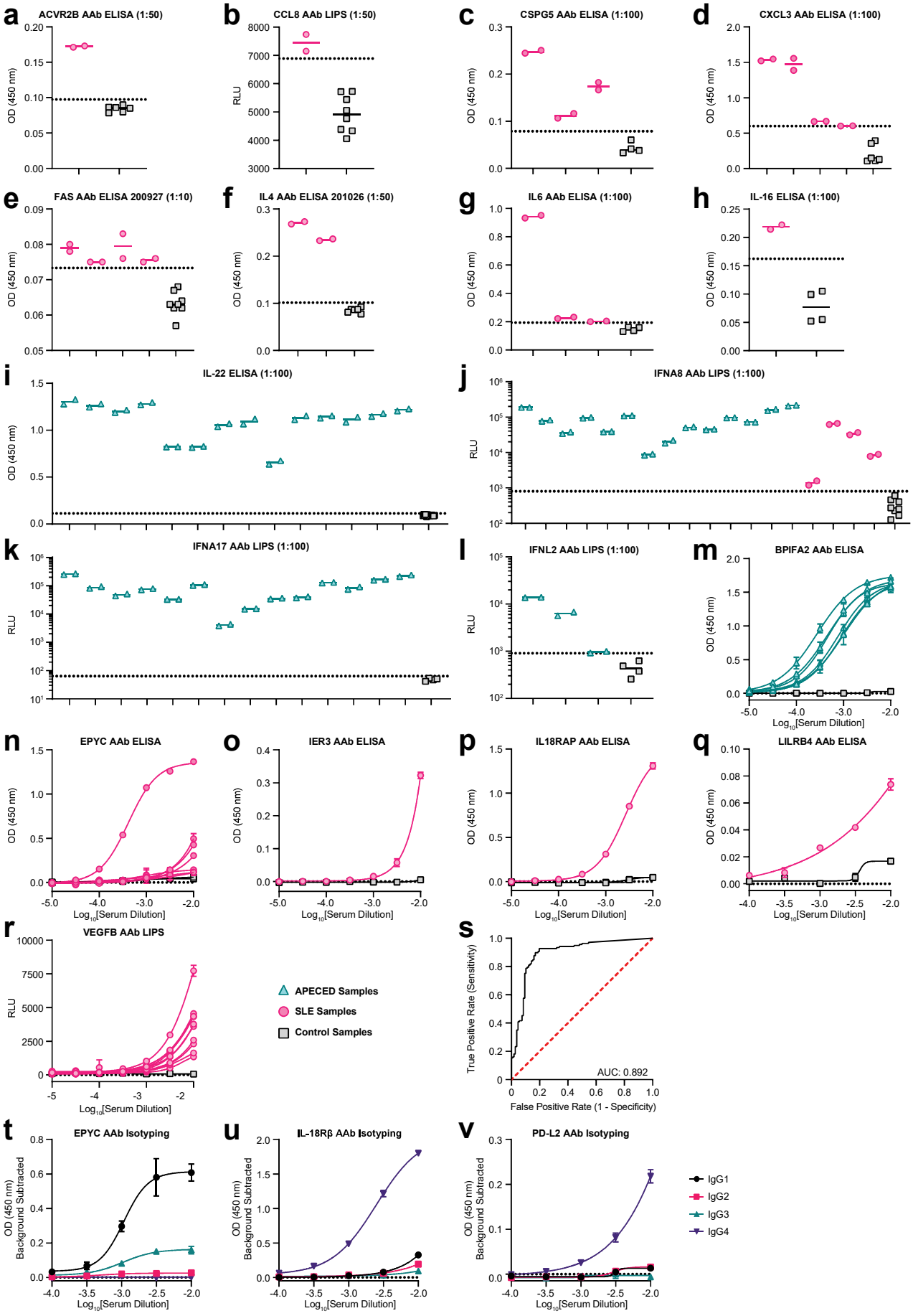

Supplementary Table 2

Supplementary Table 2 | APECED patient demographics and clinical characteristics.

APECED cohort characteristics (n = 77)	Number (%)
Age*	24 (14.4)
Gender (female)	45 (58)
Ethnicity	
White Non-Hispanic	68 (88)
White/Hispanic	5 (7)
AIRE* alleles*	
c.967_979del13	79 (51)
c.769C>T	21 (14)
Clinical manifestations	
Chronic mucocutaneous candidiasis	66 (86)
Adrenal insufficiency	62 (81)
Hypoparathyroidism	63 (82)
Hypothyroidism	18 (23)
Hypogonadism	26 (34)
Autoimmune pneumonitis	28 (36)
Autoimmune hepatitis	25 (33)
Intestinal dysfunction	53 (69)
Exocrine pancreatic insufficiency	1 (1)
Asplenia	10 (13)
Alopecia	26 (34)
Vitiligo	19 (25)
Sjogren's-like syndrome	30 (39)
Autoimmune gastritis	30 (39)
B12 deficiency	20 (26)
Intrinsic factor antibody	24 (31)
Lung-targeted autoantibodies***	
BPIFB1	19 (26)
KCNRG	4 (6)

*Age is represented as mean (standard deviation) in years
**The denominator for *AIRE* mutant alleles is 154
***Data available for 72 patients
AIRE, autoimmune regulator; APECED, autoimmune polyendocrinopathy-candidiasis-ectodermal dystrophy; BPIFB1, BPI fold containing family B member 1

Supplementary Table 3

Supplementary Table 3 | SLE patient and control demographics and clinical characteristics.

Mean (SD) or as indicated	SLE Cohort (n = 85*)	Healthy Controls (n = 20)
Age, (years)	41.7 (12.6)	37.2 (11)
Gender, N (% female)	76 (89.4)	12 (60)
Ethnicity, N (%)		
Hispanic	22 (26)	3 (15)
Non-Hispanic	35 (41)	8 (40)
African American	28 (33)	9 (45)
Clinical Manifestations, N (%)		
Skin	40 (47.1)	
Mucocutaneous	16 (18.8)	
Musculoskeletal	29 (34.1)	
Renal	20 (23.5)	
Cardiorespiratory	4 (4.7)	
Hematological	7 (8.2)	
Neuropsychiatric	0 (0)	
Serologies, N (%)		
Positive dsDNA	40 (47.1)	
Low complement	34 (40)	
SLEDAI score	6.3 (6.1)	
Medications, any use N (%)		
Prednisone	40 (47.1)	
Hydroxychloroquine	72 (84.7)	
Mycophenolate mofetil	24 (28.2)	
Methotrexate	6 (7.1)	
Azathioprine	4 (4.7)	
Belimumab	6 (7.1)	
Others (cyclophosphamide, rituximab, tacrolimus, infliximab, etc.)	10.6%	

Abbreviations: SLEDAI (Systemic Lupus Erythematosus Disease Activity Index).
Prednisone dosing ranges from 5 mg daily to 60 mg daily.
*Complete clinical data was not available for a subset of patients. A total of 106 patients were screened.